Paper III

Polyphase metamorphism in the Kalak Nappe Complex, northern Scandinavian Caledonides: implications for the history of the Baltican margin prior to and during Caledonian continental collision

Carly Faber[1], Holger Stünitz[1], Deta Gasser[2,3], Petr Jeřábek[4], Katrin Kraus[1], Jiří Konopásek[1]

[1]Department of Geosciences, UiT The Arctic University of Norway, Tromsø, N-9037, Norway
[2]Western Norway University of Applied Sciences, Sogndal 6851, Norway
[3]Geological Survey of Norway, Trondheim 7491, Norway
[4]Institute of Petrology and Structural Geology, Charles University, 128 43 Praha 2, Czech Republic

*corresponding author (e-mail: carlyfaber1@gmail.com)

Abstract

This study investigates polyphase metamorphism in the pervasively deformed Kalak Nappe Complex (KNC) and discusses the evolution of the pre-Caledonian Baltica margin Caledonian continental collision in northern Norway. The western part of the KNC was mapped and two main amphibolite facies nappes were identified and tectonostratigraphically correlated across the area. At least two phases of pre-Caledonian metamorphism and deformation can be identified, each in the different nappes ($S1^S$ in the lower nappe and $S1^E$ in the upper nappe), indicating different pre-Caledonian evolutions for the upper and lower KNC. Metamorphic conditions for the $S1^S$ event in the lower nappe are established, using phase equilibrium modelling, at lower-amphibolite facies regional metamorphic conditions (~530 – 570 °C and 8.2 – 9.3 kbar), and may be attributed to the Grenvillian/Sveconorwegian orogeny. Field evidence for the $S1^E$ foliation in the upper nappe is widespread. This foliation is the same as the granulite facies S1 foliation described by Gasser et al., (2015) dated at ~700 Ma. A pre-Caledonian high-temperature, low-pressure event is recorded along the boundary between the upper and lower nappes and may be related to the juxtaposition of the upper and lower KNC either at ~700 Ma or ~600-560 Ma, or during a yet undated event. A pervasive S2 foliation affects the entire complex, and is associated with Caledonian SE-directed thrusting. Phase equilibrium modelling was applied to tectonostratigraphically significant samples to determine the variation in S2 metamorphism throughout the complex and within the different nappes. In the lower nappe both high-temperature, low-pressure

conditions followed by higher pressure, lower temperature conditions are associated with S2 garnet growth, indicating a two-phase Caledonian evolution along an anticlockwise P-T path, similar to that observed in the overlying Reisa Nappe Complex. P-T conditions for S2 shearing along nappe boundaries increase upwards, indicating an inverted metamorphic gradient. Variation in pressure within the nappes likely reflect temporal variation, and higher pressure estimates in the internal part of the lower nappe relative to the upper nappe probably reflects underthrusting of the upper nappe by the lower nappe during crustal thickening.

1. Introduction

Determining the timing, relationship, and interaction of metamorphic and deformation events within orogenic belts is key to understanding their evolution. It gives insight for tectonic models and into the important processes that facilitate the building of continental crust. Modern continental collision zones, such as the Himalaya and the Alps, form complex mountain belts constructed from pre-existing continental crust, rocks of the intervening ocean basins, and rocks generated in local transient settings related to the collision (e.g. Yin and Harrison, 2000; Schmid et al., 2004). Continental collision usually involves re-working of pre-existing continental crust within nappes thrust over the continental margin (e.g. Escher et al., 1993; Escher and Beaumont, 1997). Events prior to final continental collision can establish structural heterogeneities, modify water content, generate migmatisation, and adjust mineral assemblages. These processes can influence the behaviour of continental crust during subsequent deformation (e.g. Austrheim, 1991; Rosenberg et al., 2005). Therefore, establishing the timing and nature of events that have affected continental crust prior to orogenesis is crucial to understanding the processes and dynamics during continental collision.

In Scandinavia, the Caledonides offer a deeply-eroded example of an Himalaya-style orogen. Silurian-Devonian continental collision between Baltica and Laurentia led to thrusting of para-autochtonous and allochthonous nappes eastward over Baltica, and re-worked continental crust is exposed in the lower nappes (Stephens and Gee, 1989; Roberts, 2003). The Kalak Nappe Complex (KNC) forms a major allochthonous nappe

pile consisting of several different nappes telescoped onto Baltica during the Caledonian Orogeny. The included crustal rocks have previously been affected by several Neoproterozoic events (Daly et al., 1991; Kirkland et al., 2005, 2006a, 2007a; 2007b, 2016; Corfu et al., 2007, 2011; Gasser et al., 2015). Its origin is debated as either: 1) the re-worked pre-Caledonian margin of Baltica (Roberts and Sturt, 1980; Zhang et al., 2016; Gee et al., 2017), or 2) an exotic terrane accreted to Baltica during or prior to the Caledonian orogeny (Kirkland et al., 2005, 2006a, 2007a, 2008b; Corfu et al., 2007, 2011). Establishing its pre-Caledonian and Caledonian metamorphic and structural evolution is complicated as minerals and outcrops can record several phases of deformation and metamorphism. In addition, the KNC is composed of several units that are comprised of different rock types, display different metamorphic grades (from lower greenschist to upper amphibolite facies), and which show different pre-Caledonian histories (e.g. Kirkland et al., 2005) indicating that the KNC is comprised of several nappes that underwent different evolutions both prior to and during the Caledonian orogeny. This work examines the western part of the KNC in northern Troms (Figs. 1, 2), and will gain insight into the metamorphic evolution of the KNC using phase equilibrium modelling of tectonostratigraphically and structurally constrained samples in order to better understand the role of the KNC and the effect of pre-Caledonian events during Caledonian continental collision.

2. Geologic background

The Caledonian mountain belt in Scandinavia is comprised of a series of allochthons originating at the Baltican margin, from within the Iapetus-realm, and as part of Laurentia (Stephens and Gee, 1985, 1989). The Kalak Nappe Complex (KNC) has generally been considered as re-worked margin of Baltica, although this is debated (e.g. Stephens and Gee, 1985; Roberts, 2003; Andréasson et al., 2009; Kirkland et al., 2006a; Corfu et al., 2007).

2.1 Geology of the Kalak Nappe Complex

The KNC outcrops over a large portion of northern Norway (Troms and Finnmark), where a section through the Caledonian nappe stack is exposed (Fig. 1; Ramsay et al.,

1985). The Baltican basement, with its autochthonous metasedimentary cover, is overlain by the parautochthonous Gaissa and Laksefjord nappe complexes (Fig. 1; Roberts, 1985; Sundvoll and Roberts, 2003). The KNC overlies these nappes, and is in turn overlain by the allochthonous metasedimentary and metaigneous rocks of the Reisa/Magerøy Nappe Complex (RNC). The Lyngsfjellet Nappe Complex, comprised of ophiolitic rocks and lower-grade metasediments, overlies the RNC and represents the only oceanic rocks in northern Norway (Fig. 1; Andresen, 1988; Kvassnes et al., 2004; Augland et al., 2014). The KNC is most studied in Finnmark, where pervasive ductile deformation attributed to Caledonian nappe stacking overprints several pre-Caledonian (1000 – 500 Ma) orogenic and intrusive events (Daly et al., 1991; Kirkland et al., 2005, 2006a; Roberts et al., 2006; Corfu et al., 2007, 2011; Zhang et al., 2016).

The KNC is comprised of ortho- and paragneisses, psammitic and pelitic metasediments, minor schists and marbles, and mafic and felsic intrusives (Andresen, 1988). Between 5-10 individual thrust sheets or nappes have been established. They are broadly separated into upper and lower KNC nappes based on their inclusion of two different sedimentary successions (Fig. 1; Gayer et al., 1985; Kirkland et al., 2006a, 2007a; Corfu et al., 2011). The Sværholt succession is recognized in the lower nappes, which also include the Fagervik Complex (Fig. 1). The Fagervik Complex consists of paragneisses deposited after 1948 ± 17 Ma intruded by granite at 1796 ± 3 Ma, ages consistent with its origin as Baltica basement (Kirkland et al., 2008b). The metasediments of the Sværholt succession were deposited between 1030-980 Ma and metamorphosed, deformed, and intruded by granitic plutons at c. 980-960 Ma (Grenvillian/Sveconorwegian; Kirkland et al. 2006a, 2007b, 2008b; Corfu et al., 2011). They are in tectonic contact with the underlying Fagervik complex, and their detrital zircon profile suggests they were not sourced from Fagervik-type rocks (Akselsen, 1982; Kirkland et al., 2007b, 2008b). The upper nappes of the KNC contain paragneisses and metasediments of the Sørøy succession (Fig. 1), deposited between 910-840 Ma and deformed, metamorphosed and intruded by granitic rocks at c. 850-820 Ma and c. 710 Ma (Kirkland et al., 2006a; 2007a, 2007b, 2008b; Corfu et al., 2007, 2011). The Sørøy succession was also intruded by the mafic and ultramafic rocks of the Seiland Igneous Province (SIP), and locally migmatised between

580 – 560 Ma, with late magmatism at 520 Ma (Fig. 1; Roberts et al., 2006, 2010). A minor succession at the top of the KNC in Finnmark is comprised of the Falkenes limestone and Åfjord pelite, deposited between 760-710 Ma (Kirkland et al., 2006a; Slagstad et al., 2006).

Caledonian shearing and metamorphism are responsible for the majority of the deformation in the KNC, and rocks are strongly and pervasively deformed. Primary relationships are therefore difficult to establish (Ramsay et al., 1985; Dallmeyer, 1988). Caledonian metamorphic grade in the KNC increases from low- to mid-greenschist facies at the base in the east to upper-amphibolite facies at the top in the west, indicating it must be comprised of several thrust sheets of different metamorphic grade (Roberts, 1985; Rice, 1984, 1985, 1987). At least two pre-Caledonian events in the upper part of the complex (Sørøy succession) have imposed granulite facies conditions on the rocks (migmatisation at ~700 Ma and contact metamorphism related to SIP intrusion at 580-560 Ma; e.g. Elvevold et al., 1993, 1994; Menegon et al., 2011; Gasser et al., 2015; Kirkland et al., 2016). The metamorphic conditions and context of pre-Caledonian events in other parts of the complex are not well understood.

Two to five deformation events are described in the KNC (Gayer et al., 1985). The following four are most important: 1) a biotite-grade metamorphic foliation that pre-dates ~980 Ma granitic intrusives in the lower units of the KNC, 2) porphyroblasts and tectonic lenses that preserve a migmatitic foliation (steeply-dipping) formed at ~700 Ma in the upper KNC, 3) a steeply-dipping migmatitic foliation associated with contact metamorphism during intrusion of the SIP in the upper KNC, 4) a strong pervasive gneissic to mylonitic foliation, typically considered as the most prevalent deformation phase, and associated with Caledonian shearing (Kirkland et al., 2005, 2006a; Menegon et al., 2011; Gasser et al., 2015). The age of Caledonian metamorphism and shearing is recorded between 440 – 425 Ma (Rice and Frank, 2003; Kirkland et al., 2007a, 2008a; Corfu et al., 2011; Gasser et al., 2015). Emplacement direction of the nappes is mainly SE-directed with late east-directed movement (Townsend, 1987; Gayer et al., 1987, Gasser et al., 2015). Several folding events are described with the oldest prior to intrusion

of ~980 Ma granites in the lower nappes. Recumbent isoclinal folding is generally associated with Caledonian nappe emplacement (Ramsay et al., 1985; Daly et al., 1991). The youngest folding occurs as upright, symmetrical, open folds and a local crenulation cleavage (Gayer et al., 1985).

2.2 Previous work in the study area

The study area comprises the western extent of the KNC in northern Troms along the Norwegian coast, and includes parts of the mainland and several islands (Uløya, Kågen, Skjervøy, and Arnøya). Pre-Caledonian migmatisation in the rocks at Eide and on southern Skjervøy (Sandøra gneiss; Fig. 2) is dated at 702 ± 5 Ma and 706 ± 3 Ma, respectively, and records metamorphic conditions of 760-775 °C and 8.8-9.8 kbar (Corfu et al., 2007; Gasser et al., 2015). Caledonian metamorphism at Eide is estimated at 600-660 °C and 10-12.5 kbar and occurred over at least 10 Ma between 440 - 430 Ma, possibly continuing to 420 Ma (Gasser et al., 2015). Immediately south and east of the field area the Corrovarre Nappe is found below the RNC (Fig. 1). Here it is described as the highest unit in the KNC, and considered a possible correlative of the Sørøy succession. Previous maps have considered the entire KNC in the field area as part of the Corrovarre nappe (Zwaan, 1988; Zwaan and van Roermund, 1990; Lindahl et al., 2005; Gee et al., 2017). The Corrovarre nappe is intruded by abundant metadolerites and some larger mafic bodies with tholeiitic compositions (Roberts, 1990). Zwaan and van Roermund (1990) estimated metamorphic conditions related to the contact metamorphism of the mafic rocks at ~850 °C at 5.5-6.5 kbar, followed by kyanite-present Caledonian shearing at higher pressures and lower temperatures. Recent work has dated granite associated with contact metamorphism of the mafic dykes in the Corrovarre nappe at 610.2 ± 1.1 Ma (Gee et al., 2017).

3. Field observations

The map of the studied region (Fig. 2) was produced using a combination of fieldwork and existing map material (Roberts, 1973; Zwaan, 1988). Several areas were investigated in detail, including Straumfjord, Eide, and Uløya. Previous mapping in the northern part of the field area did not correlate well with the southern part, and therefore Arnøya and

Skjervøy were also considered in detail. The KNC in the study area comprises at least three thrust sheets or nappes.

3.1 Lithologies and tectonostratigraphy

3.1.1 Lowermost units

Greenschist facies metasediments comprise the lowermost units around Rotsundelv and on the eastern side of Reisafjord (Fig. 2). They are composed predominantly of fine-grained meta-arkose and often contain chlorite and epidote. These greenschist facies metasediments are separated from overlying orthogneiss by a greenschist-facies mylonitic zone.

3.1.2 Lower units

The orthogneiss forms the base of the main lower nappe. It is granodioritic in composition and occurs mainly around the southern-most parts of Reisafjord and on southwestern Arnøya. The lower part of the orthogneiss displays local greenschist-facies metamorphism within shear zones (e.g. Fig. 3A). The upper part of the orthogneiss unit, exposed around Straumfjord and on Arnøya, is amphibolite facies and often strongly sheared. It is usually found as quartz-feldspar mylonite. In its upper part, layers of amphibolite and hornblende schist are folded together with the orthogneiss (e.g. Straumfjord; Fig. 2, 3B, 3D, 4). At Hamneide the amphibolite and horblende schists dominate and contain lenses of orthogneiss (Fig. 4). The orthogneiss also includes rare small (10-40 m) lenses of clinopyroxene gabbro of unknown age or origin. Based on the difference in metamorphic grade between the upper and lower parts of the orthogneiss the rocks probably comprise at least two different nappes, however a clear jump in metamorphic grade was not observed. The deformation is extremely pervasive so that individual nappes are difficult to distinguish in the field.

On Skjervøy the lower units are comprised of mainly amphibolite-facies marble and amphibolite with calc-schist that grades upwards into a garnet-mica-schist and amphibolite unit (Figs. 2, 3C, 4). In low strain zones garnet amphibolite layers crosscut an earlier foliation in the garnet-mica-schists, suggesting an intrusive relationship. On

Skjervøy, meta-arkose occurs as the middle unit (Figs. 2, 4). This unit is similar to the uppermost unit of the lower KNC elsewhere in the study area (e.g. Straumfjord), which is comprised of meta-arkose with mafic layers and lenses and occasional layers of mica-schist (Fig. 3E). On Skjervøy the lower boundary of the meta-arkose unit with the garnet-mica-schist and amphibolite rocks is usually mylonitic, although in lower strain zones they are folded together. The meta-arkose unit is pervasively sheared under amphibolite facies conditions and contains granitic lenses and garnet amphibolite layers parallel to the foliation (Fig. 3E). As there are multiple meta-arkose units at different levels in the KNC (e.g. Fig. 4) this meta-arkose unit is referred to as the lower meta-arkose.

3.1.3 Upper units

The upper part of the KNC, mainly at Eide, on Uløya, and Arnøya (Fig. 2), is comprised of a sequence of paragneisses, amphibolite and hornblende schists with garnet metapsammites, and meta-arkose with garnet-mica-schist (Figs. 2, 4, 5A-F). The rocks all display at least amphibolite facies metamorphism. The paragneisses are generally metapelitic to metapsammitic, and are interlayered with garnet-amphibolite and garnet-mica schist. They are pervasively sheared and zones with abundant quartz-feldspar porphyroclasts are common (e.g. Fig. 5A). The paragneisses also contain layers and lenses of migmatitic gneiss (e.g. Eide, Skjervøy; Figs. 2, 4; 5B; described previously at Eide; Gasser et al., 2015). Amphibolite layers also contain leucosome, indicating that they probably underwent minor partial melting (Figs. 5C, D). The uppermost unit of the KNC is a meta-arkose and garnet-mica-schist with minor amphibolite layers. This unit is usually strongly sheared and occurs locally on Uløya, Kågen Hamneide, Arnøya, and uppermost Straumfjord (Figs. 2, 4, 5E). Occasionally cm-scale sheared felsic layers and lenses and pegmatites occur (Fig. 5E). This meta-arkose unit is referred to as the upper meta-arkose.

3.2 Structures

3.2.1 Caledonian fabrics

There is a single dominant mylonite foliation and lineation in the whole study area. These fabric elements can always be correlated everywhere and constitute the S2 and L2, i.e. a

transposed foliation and stretching lineation. The relative timing of the formation of this S2 fabric is Caledonian. The pervasive S2 mylonitic foliation is near horizontal or dips shallowly towards the SE or NW throughout most of the area (Figs. 6B-E; red dots are poles to S2 foliation). In Straumfjord the S2 foliation is mostly horizontal or shallowly SW- or NE-dipping (Fig. 6A). The S2 foliation is always associated with a strong stretching lineation (L2) that plunges shallowly SE or NW throughout most of the area (Figs. 6A-F). In the lower KNC nappes in Straumfjord and northern Skjervøy (Figs. 6A, B) some stretching lineations show a more ESE and eastward trend, whereas within the upper nappes at Eide and on Uløya (Figs. 6D, E) the stretching lineation tends towards a more SSE and southward trend. The L2 lineation is always associated with top-to-SSE/SE/ESE shear sense indicators.

3.2.2 Folding

Folding in the KNC in the study area is rare, but does occur on several scales. Regardless of their generation, folds almost always have axes trending NW-SE with horizontal axial planes approximately parallel to S2 (Figs. 6A-F). In both the upper and lower parts of the KNC older foliations are folded into recumbent isoclinal folds, usually with sheared off limbs (Figs. 3D, 5D, F). In the lowest strain domains in the lower units folds sometimes have a greater interlimb angle and fold axial planes are more steeply-dipping. Examples occur in the lower KNC rocks in Straumfjord, on northern Skjervøy, and within the lower meta-arkose unit, where metre-scale closed to tight folds that plunge shallowly towards the SE have steeply to moderately inclined SW-dipping axial planes (mostly SW-dipping; e.g. Figs. 3C, G, 6A, B). Of the folds that have this geometry, two types occur: 1) amphibolite facies (garnet present) rocks with an axial planar foliation in schistose units (e.g. Fig. 3C), and 2) folding of a lower-grade (garnet absent) foliation (e.g. Figs. 3F, G). In some cases the type 2 folds are re-oriented (axial planes are near horizontal; e.g. Fig. 3F), or they have axial planes that are gently folded (e.g. Fig. 3G) prior to being crosscut by pegmatitic granitic magmatism and fine-grained mafic dykes. Sometimes the intrusives display a weak foliation parallel to S2. This indicates that folds with the same geometry may have formed during different metamorphic events in the lower KNC. In the lower KNC the orthogneiss and mafic rocks are folded together in large 100m-scale folds

that are isoclinal and recumbent with NW-SE trending axes (Fig. 6A; red box) and a near horizontal axial plane. In some cases fold hinges preserve an earlier S1 foliation, which is recognized based on a clear difference in metamorphic grade with respect to the S2 foliation. A well-exposed example in Straumfjord displays a lower-grade, lower-strain S1 foliation (Figs. 3B, D, 6A; orange dots) preserved in the hinge zone of a 100 m-scale isoclinal recumbent fold (S2; Fig. 6A; red dots).

In the upper units of the KNC (paragneisses, amphibolites and meta-arkoses) early low-grade folds that are crosscut by pre-Caledonian intrusives (such as on Skjervøy) and folds that preserve a lower grade foliation in their fold hinges (such as those in Straumfjord), were not observed. Folding is usually tight to isoclinal with horizontal or shallowly NW or SE-dipping axial planes, parallel to the S2 foliation. Fold axes generally plunge towards the SE, parallel to the L2 lineation, although there is some variation (Figs. 5D, F, 6C-F). On southern Skjervøy (upper KNC: Fig. 6C) they trend towards E and SE, whereas at Eide and on Arnøya they trend more towards the SSE and S (Figs. 6D, F). On Uløya they vary between E-, SE and S-trending. The folded rocks in the upper KNC generally display amphibolite facies conditions, although a rare earlier migmatitic foliation is observed within dismembered fold hinges and tectonic lenses in the paragneisses (Figs. 5B, 6C, D, E).

3.2.3 Pre-Caledonian fabrics

Several pre-Caledonian foliations are observed in the KNC in the study area: 1) The orthogneiss and mafic rocks in Straumfjord preserve an early lower-grade steeply-dipping, and occasionally folded foliation that contains epidote and amphibole and lacks garnet (Figs. 3B, D, 6A, B). 2) In low strain zones within the lower meta-arkose an early, lower-grade (no garnet), steeply-dipping or folded foliation is crosscut by pegmatitic granitic intrusions (Fig. 3F) and fine-grained mafic dykes (Fig. 3G). 3) In the upper KNC a pre-Caledonian migmatitic foliation often preserves higher-grade conditions (granulite facies) than the overprinting amphibolite-facies Caledonian S2 foliation (Figs. 5B, 6C, D, E).

The relative timing of these pre-Caledonian foliations is unclear as they occur within at least two different nappes. They are therefore described here as S1, but differentiated using superscript letters. The lower-grade S1 foliation in the lower KNC, preserved around Straumfjord and in the lower units on Skjervøy is referred to as $S1^S$, whereas the migmatitic S1 foliation visible in lenses on southern Skjervøy and around Eide is referred to as $S1^E$. In Straumfjord $S1^S$ is preserved as a steeply to moderately SW- to NE-dipping foliation in the orthogneisses and amphibolite rocks (Figs. 3D, 6A). It is also associated with a weak vertical to steeply NE-plunging stretching lineation. Based on the lack of garnet in the quartzofeldspathic and amphibolite rocks, and the presence of epidote in the amphibolites, its metamorphic grade is probably lower amphibolite facies. At transitions to the Caledonian S2 foliation (e.g. Fig. 3B) garnet appears and epidote disappears. On northern Skjervøy the $S1^S$ in mica-schists is crosscut by mafic intrusions, and in the lower meta-arkose unit the $S1^S$ foliation is either steeply SW-dipping or folded, with folds crosscut by mafic and felsic intrusions (as previously described; Figs. 3F, G). The $S1^E$ foliation occurs within lenses in the paragneisses of the upper KNC (Fig. 5B). It is associated with garnet, biotite, and kyanite, and has previously been described by Gasser et al., (2015). In the upper meta-arkose the $S1^E$ foliation is present in outcrop-scale low-strain lenses and sometimes preserves folding with axial planes parallel to S2 (Fig. 5F).

4. Tectonostratigraphic correlation

The greenschist facies meta-arkoses in Straumfjord form a clear lowermost nappe in the area (Figs. 2, 4). The rest of the KNC is assigned to two main laterally extensive nappes based on their lithology, local tectonostratigraphic position, and pre-Caledonian structures (Fig. 4). The orthogneisses and amphibolite and hornblende schists in Straumfjord, on Arnøya, and Hamneide form the lowermost part of the KNC, and are folded together. Although orthogneiss is not present on lowermost Skjervøy, the presence of the $S1^S$ foliation in the lower Skjervøy units and the lower meta-arkose suggests that these rocks are at a similar tectonostratigraphic level (Fig. 4). Based on a similarity in pre-Caledonian structures and metamorphic grade, the lower meta-arkose unit on Skjervøy probably correlates with meta-arkose that overlies the orthogneiss south of Rotsundelv and Sørkjosen, and which occurs as a thin (<100 m-thick) sliver below the migmatitic gneiss

at Eide. Therefore, the lower part of Skjervøy is grouped with the lower units in Straumfjord, Eide, Hamneide and Arnøya as part of a lower nappe in the field area. The increase in metamorphic grade from greenschist facies in the lower part of the lower KNC unit to amphibolite facies in the upper part of this unit suggests that the lower part of the KNC in the area comprises at least two different nappes.

The upper KNC nappe in the field area is comprised of the paragneisses with interlayered amphibolite and garnet-mica-schist, including layers and lenses of migmatitic gneiss (preserving $S1^E$; Fig. 4). This unit forms a thin layer in the upper part of Straumfjord, Hamneide, and occurs as pervasively sheared rocks with rare preserved layers and lenses of migmatitic gneiss at Eide, on lower Taskeby, and on upper Skjervøy. This unit also forms the majority of the KNC rocks on Arnøya (Fig. 4). The upper meta-arkose, amphibolite and mica-schist unit overlies the paragneisses and forms the uppermost part of the KNC tectonostratigraphy in the area, at Hamneide, on Uløya, at Taskeby, on Kågen, and as a thin layer locally present on southern Arnøya. The amphibolite and garnet-mica-schist that occurs at the top of Eide are similar to the amphibolite layers within the upper meta-arkose elsewhere, and is therefore tectonostratigraphically equivalent to the uppermost part of the nappe. The migmatitic gneisses sometimes also occur as layers or lenses immediately below the KNC-RNC boundary, probably as a thin thrust slice (e.g. Uløya and Arnøya; Fig. 4). Together, the paragneiss and upper meta-arkose units form the upper unit in the field area. Because the rocks display the same metamorphic grade and pervasive deformation, it is unclear if this unit is comprised of one or several nappes.

5. Analytical methods

Bulk rock X-ray fluorescence analyses were performed with a Panalytical Axios XRF spectrometer at the University of Cape Town, South Africa. Analyses for eleven major elements (Fe, Mn, Ti, Ca, K, S, P, Si, Al, Mg, and Na) were performed on fused disks prepared with a lithium borate flux. Loss on ignition (LOI) was determined from weight loss of the samples after 1.5 h ignition at 1050 °C (Table 2). Compositions for garnet, biotite, feldspar, and white mica (Tables 3 and 4) were measured using two instruments.

For samples ST257, S8d, S174a, and S17 a JEOL JXA-8100 electron microprobe at the University of Cape Town was used. Analyses were carried out using a 15 kV accelerating voltage, 20 nA probe current and 2-3 μm spot size. Counting times were 5 seconds for background and 10 seconds for peaks on all elements. Data were processed using ZAF matrix corrections and reduced with the PAP procedure. Mineral compositions in sample UL250 were measured on a JEOL JXA-8900R electron microprobe at the Christian-Albrechts University in Kiel, Germany. Analyses were carried out using an accelerating voltage of 15 kV and beam current of 15 nA. Counting times for background was 7 seconds and for peaks was 15 seconds. Garnet, biotite and muscovite were measured with a fully focused beam of 1 μm diameter and feldspar was measured with a 5 μm beam. Matrix corrections were carried out according to the CITZAF procedure version 3.5 in the JEOL software. The garnet map for sample UL250 was produced by dividing the mapped area into a grid of measuring points on which counting rates were generated to obtain relative element concentrations. Microprobe analyses of amphibole in samples ST254b and ST257 were re-calculated based on 13 cations plus Ca, Na, and K (i.e. no Mg/Fe/Mn on the M4 site). Mineral abbreviations are according to Whitney and Evans (2010).

6. Petrography and mineral chemistry

6.1 Lower KNC - Straumfjord

Both the pre-Caledonian $S1^S$ foliation and the S2 foliation were sampled and investigated. Sample ST254b is an amphibolite, representative of the $S1^S$ foliation. It was taken from the hinge zone of a 100 m-scale isoclinal recumbent fold (Table 1; Figs. 2, 3D, 4). Sample ST257 is a garnet amphibolite, representative of the S2 foliation. It was taken from the sheared lower fold limb of the same fold (Table 1; Figs. 2, 3B, D, 4). The samples were taken approximately 200 m apart.

6.1.1 $S1^S$ foliation – ST254b

Sample ST254b is a medium-grained amphibolite containing epidote, zoisite, quartz, calcite and titanite. Amphibole grains define the $S1^S$ foliation. Titanite is abundant and forms elongate grain clusters parallel to the $S1^S$ foliation (Fig. 7A). Calcite mainly occurs with quartz. Two amphibole populations occur: 1) as rounded or equant porphyroclasts

surrounded by a thin, often sigmoid-shaped mantle of quartz, epidote and sometimes calcite and younger amphibole, and 2) as elongate grains parallel to $S1^S$ (Fig. 7A). The asymmetry of the sigmoid structures indicate an ambiguous shear sense. The two amphiboles display slightly different compositions. Early amphibole at the core of sigmoid structures has a magnesio-hornblende composition, whereas younger prismatic amphibole has a more tschermakitic hornblende composition (Table 4).

6.1.2 S2 foliation – ST257

Sample ST257 is a medium-grained garnet amphibolite with a strong L2 stretching lineation defined by amphibole. The S2 foliation is defined by amphibole and biotite. Garnet forms abundant inclusion-rich, euhedral, 0.05 – 0.3 cm-sized porphyroblasts (Figs. 7B, C). Plagioclase and quartz occur as elongate grains in the matrix. Clinopyroxene is found as rare inclusions in garnet cores (Fig. 7C). Calcite is relatively common (~5-10 modal%) and is found as inclusions in garnet rims and along garnet grain boundaries, it is also often intergrown with amphibole and quartz, and overgrows plagioclase in the matrix (Fig. 7B). Biotite is intergrown with amphibole. Ilmenite is abundant and occurs as inclusions in garnet rims and in the matrix (Fig. 7C). Minor rutile is also found in the matrix. Some garnet grains show S-shaped inclusion trails consistent with top-to-SE shearing. Garnets display zoning with X_{Mg} content lower in garnet cores (as low as 0.13) than rims (up to 0.16), grossular and almandine are slightly lower in cores (Alm_{53-56} and Grs_{19-21}) than rims (Alm_{56-59} and Grs_{20-23}), and spessartine content is higher in garnet cores (Sps_{8-15}) than rims (Sps_{3-5}) (Table 2). Zoning across garnet is gradual (Fig. 8A). Plagioclase displays an oligoclase composition (An_{17-19}). Biotite has an X_{Mg} between 0.52-0.55, and amphibole has a tschermakitic composition (Table 4).

6.2 Lower KNC - amphibolite and mica-schist unit, Skjervøy (S8d)

Sample S8d comes from Skjervøy from the lower part of the KNC (Table 1; Figs. 2, 4). The sample is a medium-to fine-grained garnet-mica-schist with a well-defined S2 foliation (Fig. 7E). Garnet occurs as 0.1-0.5 cm-sized subhedral porphyroblasts with abundant inclusions. Inclusions record an earlier planar foliation that has been variably rotated with respect to S2. Chlorite, ilmenite and biotite occur as inclusions (Fig. 7D).

Quartz mantles with sigma geometry around garnet porphyroblasts indicate top-to-SE shear sense. The strong S2 foliation in the sample is defined by muscovite, biotite, quartz ribbons and elongate quartz-plagioclase aggregate layers. Muscovite is the dominant mica (Fig. 7E). Ilmenite is the dominant titanium-bearing phase in the matrix, although rutile does occur. Garnets show distinctive zoning (Fig. 8B). Inclusion-poor core zones have a lower X_{Mg} content and higher Grs composition in cores (X_{Mg}= 0.06-0.13, Grs_{9-15}) than rims (X_{Mg}=0.14-0.16, Grs_{5-7}; Table 2). Zoning in Sps content also occurs, but its peak values have no relationship with the microstructure of the garnet (Fig. 8B). Highest Sps values occur in the middle of the grains (up to $Sps_{3.5}$) and decrease towards the rims (~Sps_1). Feldspars have a composition between An_{16-19}, X_{Mg} content in matrix biotite is between 0.43-0.5, and Si content in white mica is between 3.03-3.14 (a.p.f.u.; Table 4).

6.3 Lower KNC - lower meta-arkose unit, Skjervøy (S174a)

Sample S174a is medium-grained garnet-biotite-gneiss from the upper part of the meta-arkose unit on Skjervøy (lower meta-arkose; Table 1; Figs. 2,4). The sample contains abundant 0.1-0.4 cm-sized sub- to euhedral garnet porphyroblasts in a matrix of biotite, plagioclase and quartz. It preserves a moderate S2 foliation, defined by biotite, elongate quartz and abundant plagioclase. Garnet porphyroblasts with biotite tails display a sigma geometry indicating a top-to-SE shear sense. Garnet grains contain inclusions with garnet cores rich in fine-grained inclusions and rims containing slightly larger inclusions (Fig. 7F). Titanite is abundant in the matrix and occurs as sub- to euhedral grains parallel to the foliation (Fig. 7G). Minor ilmenite is found as inclusions in garnet. Larger inclusions in the mid- to rim regions of garnet are chlorite and zoisite (Fig. 7F). The garnet profile shows a core a rim structure in the garnet grains, and compositional trends change across the garnet profile (Fig. 8C). Almandine is high in the cores (Alm_{57-59}), decreases to Alm_{46-49} in the mid-garnet and then increases towards the rims (Alm_{55-58}). Grossular in garnet cores is between Grs_{22-29}, increases in the mid-garnet to Grs_{35-37} forming an almost flat profile that decreases slightly towards the rims (Grs_{34-36}). X_{Mg} content is higher in the cores (0.06-0.07), decreases in the mid-garnet to 0.03-0.04, and increases steadily towards the rims (0.06-0.07). Sps content is between Sps_{7-11} in the cores, increases in the mid-garnet to Sps_{14-15}, and decreases steadily towards the rims (Sps_{1-2}) (Table 3; Fig. 8C).

Plagioclase has a composition of An_{19-23}, with rims displaying the higher anorthite content, and biotite has an X_{Mg} content of 0.29-0.32 (Table 4).

6.4 Upper KNC – parageneiss unit, Kågen (S17)

Sample S17 is a coarse-grained garnet-kyanite-staurolite-gneiss from the KNC on the island of Kågen ~200 m below the boundary with the Vaddas nappe (Table 1; Figs. 2, 3). It is a coarse-grained rock with 0.1-0.3 cm-sized subhedral garnet porphyroblasts, 0.05-0.2 cm staurolite porphyroblasts, and 0.2-0.4 cm poikilitic porphyroblasts of kyanite in a matrix of quartz, feldspar and muscovite (Figs. 7H, I). Muscovite, staurolite and kyanite define a strong anastomosing S2 foliation and muscovite fish (<0.3 cm) indicate top-to-SE shear sense. Kyanite occurs as large occasionally bent grains and as fine grains along the boundaries of staurolite grains (Figs. 7H, I). Staurolite is less abundant than kyanite and is parallel to the S2 foliation (Fig. 7H). Rutile is relatively abundant and occurs as elongate 50-200 mm-sized grains within the S2 foliation and as inclusions in kyanite, staurolite and garnet cores and rims. Although garnet grains appear to have a distinct core-rim structure with inclusion-free cores and poikilitic rims (quartz inclusions), the garnet profile is flat and garnets show no compositional zoning (Fig. 9A). Their composition is around $Alm_{65-74}Py_{15-17}Grs_{6-7.2}Sps_{2-3}$ and X_{Mg} values are between 0.18-0.20 (Table 3; Fig. 9A). Muscovite has a Si content between 3.01 and 3.14 (a.p.f.u.; Table 4).

6.5 Upper KNC - upper meta-arkose unit, Uløya (UL250)

Sample UL250 is a medium- to coarse-grained garnet-biotite-gneiss from Uløya. It comes from the upper meta-arkose unit (Table 1; Figs. 2, 3). The sample contains compositional bands richer and poorer in pelitic material. Garnet forms euhedral 0.05-0.2 cm-sized porphyroblasts often rich in inclusions. Inclusion trails in garnet porphyroblasts indicated syn- and post-tectonic garnet growth (Fig. 7J). A strong S2 foliation is defined mainly by biotite and elongate quartz and feldspar grains. Asymmetric biotite and quartz mantles around garnet porphyroblasts indicate top-to-SE shear sense. Muscovite occurs as two populations, with the majority as large, often bent fish overgrown by biotite (Fig. 7J), and as rare late grains that crosscut the main S2 foliation. Titanite is abundant and forms large (up to 0.5 mm-long) euhedral grains parallel to the foliation and inclusions in garnet (Fig.

7J). Chlorite is also found as inclusions in garnet. Garnet grains have compositionally variable zones (Table 3; Fig. 9B). Local zones within cores have a higher spessartine content (up to ~Sps_{13}) and slightly lower X_{Mg} value (0.08) than rims (Sps_{2-3} and X_{Mg} = 0.09). Grs content varies across garnet, however rims and cores have similar compositions (Grs_{23-31}) and almandine is generally higher in rims (Alm_{60}) than cores (Alm_{50}), although this is variable. Due to the complexity shown by the garnet profile, garnet mapping was used to better identify the garnet zoning microstructure. A map of Mn in garnet shows higher Mn cores and two outer defined zones with discrete boundaries of lower Mn content (Fig. 9B). The outermost zone forms a thin rim along the edge of garnet grains. Smaller garnets only show the two outermost compositions. Biotite has an X_{Mg} content between 0.35 and 0.42. Plagioclase has a composition from An_{17-28}, with rims displaying the lowest anorthite content, and Si content in muscovite is between 3.04 and 3.22 (a.p.f.u.; Table 4).

6.6 KNC-RNC boundary (AR186)

Sample AR186 is a garnet-biotite mylonite that comes from the Kalak-Vaddas boundary on southern Arnøya. Since the boundary is strongly sheared and the rocks comprising the RNC above and KNC below are both quartzofeldspathic, it is unclear whether the protolith originally formed part of the KNC or lower RNC (Table 1; Figs. 2, 3). The sample is a feldspar-rich rock with a strong mylonitic S2 foliation defined by singular biotite grains and elongate feldspar and quartz grains. Garnet forms 0.1-0.3 cm subhedral porphyroblasts with biotite tails indicating top-to-SE shear sense (Figs. 7K, L). Chlorite occurs as inclusions in garnet cores (Fig. 7K). Plagioclase and K-feldspar are abundant in the matrix, and white mica is found as fine grains overgrowing K-feldspar (Fig. 7L). Titanite is the most abundant titanium-bearing phase in the matrix, with rare rutile grains. Both form parallel to the S2 foliation. Trace amounts of epidote form on the rims of allanite grains. Although garnets have a clear core-rim microstructure, they display only minor zoning (Table 3; Fig. 9C). Almandine content is lower in cores (Alm_{54-57}) than rims (Alm_{57-60}). Grs shows a slight increase from Grs_{28} in cores to Grs_{33} in rims, and X_{Mg} values decrease slightly from core (0.05) to rim (0.04). Sps content in cores (Sps_{8-12}) is higher than in rims (Sps_{7-8}). Plagioclase has a composition between An_{9-12}, with An

content slightly higher in cores than rims, and Si content in muscovite is between 3.2-3.3 (a.p.f.u.; Table 4).

7. Phase equilibrium modelling

P–T conditions for the seven samples (described above) were estimated using phase equilibrium modelling applied with the Perple_X software (Connolly, 2005: version 6.6.6) using the internally consistent thermodynamic data set of Holland and Powell (1998: 2004 upgrade). The calculations were performed in the MnNCKFMASHTi system using XRF whole-rock compositions (Table 2). The following solution mixing models were used for pelitic and semi-pelitic samples S8d, S174a, UL250 and AR186: garnet (White et al., 2007), staurolite, chlorite, chloritoid (Holland & Powell, 1998), biotite (Tajčmanová et al., 2009), ternary feldspar (Fuhrman & Lindsley, 1988), ilmenite (ideal mixing of ilmenite, geikielite, and pyrophanite end-members), and white mica (Coggon & Holland, 2002). In addition to the above ilmenite, biotite, chlorite, garnet and feldspar models, the following models were used for modelling mafic samples ST254b and ST257: clinoamphibole (Wei and Powell, 2003; White et al., 2003), orthopyroxene, clinopyroxene, (Holland and Powell, 1996; Zeh et al., 2005), and calcite (Holland and Powell, 2003). In all samples but ST254b the Fe^{3+} content of the minerals considered is negligible and Fe^{3+} oxides occur in negligible amounts. Therefore iron was considered only as Fe^{2+}. Although sample ST254b contains epidote, the pseudosection was calculated with Fe^{2+} and zoisite was considered as a proxy for the epidote. Apatite was observed in all samples and therefore the corresponding amount of CaO bonded to P_2O_5 observed in the whole rock analyses was subtracted from the bulk compositions. Measured chemical compositions of the relevant minerals (Tables 3 and 4) were compared with model isopleths in the calculated pseudosections. Molar percent of grossular (Grs) and spessartine (Sps) end-members and the X_{Mg} (Mg/Mg + Fe_{tot}) value in garnet were used and are shown on the P-T sections. Isopleths for anorthite content in plagioclase (An = Ca/Ca + Na + K), X_{Mg} (Mg/Mg + Mn + Fe_{tot}) in biotite, and Si content in white mica were used where relevant for further constraining estimates or for checking consistency between garnet and co-existing minerals. All samples were modelled under fluid saturated conditions.

7.1 Straumfjord $S1^S$ foliation (ST254b)

The presence of calcite in the rock suggests that the metamorphic fluid was a CO_2-H_2O mixture. X_{CO2} was therefore estimated from a T- X_{CO2} section. An approximate pressure (8 kbar) was first estimated from the correspondence of the observed mineral assemblage (with the exception of calcite) with phase fields on a water saturated P-T section. X_{CO2} was then estimated to be 0.02 from the appearance of calcite with the observed mineral assemblage on the T- X_{CO2} section. The resulting P-T section (Fig. 10A) shows calcite at low temperatures, disappearing towards higher temperatures between 500-560 °C within the pressure range considered (6 – 11 kbar). The presence of amphibole, epidote, ilmenite, and abundant titanite constrain P-T broadly to 570 – 600 °C and 7.8 – 10 kbar. The presence of two amphiboles and intergrown calcite indicates equilibration around the calcite-in curve on the lower temperature side of this broad estimate (Fig. 10A). The lack of observed garnet, plagioclase and biotite in the sample indicates that it probably equilibrated in the phase field Amp-Amp-Zo-Ilm-Sph-Qtz-Grt-Bt-Pl, where zoisite acts as a proxy for epidote, and garnet, plagioclase, and biotite are predicted as only minor components of the assemblage (2-3 modal%, ~6 modal% and <3 modal%, respectively; Fig. 10A). This phase field also gives the highest modelled modal% values for titanite within the pseudosection (up to 2 modal%), which is consistent with the abundance of titanite as an accessory mineral in the sample. Therefore P-T for the formation of the $S1^S$ foliation in sample ST254b can be further constrained to 530 – 570 °C and 8.2 – 9.3 kbar (Fig. 10A).

7.2 Straumfjord S2 foliation (ST257)

Replacement microstructures suggest the sample records evolving P-T conditions. The presence of calcite in the rock (in the matrix and as inclusions in garnet rims) suggests that the local metamorphic fluid was a CO_2-H_2O mixture. X_{CO2} was therefore estimated from a T- X_{CO2} section taken at 12 kbar. Pressure for the T-X_{CO2} was estimated from the position of X_{Mg}, Grs and Sps isopleths, representing garnet rim compositions, on a water-saturated P-T section. The X_{CO2} value (0.07) was taken from the appearance of calcite together with the stable peak assemblage and a match between garnet rim compositions and modeled X_{Mg}, Sps and Grs isopleths. On the resulting P-T section (Fig. 10B)

modelled isopleths for garnet cores correspond well with measured compositions in the Grt-Bt-Amph-Pl-Ilm-Cpx-Qtz phase field at 675 – 690 °C and 8.3- 9 kbar, consistent with the presence of clinopyoxene inclusions in garnet cores (Fig. 7C). Higher Grs and X_{Mg} and lower Sps compositions towards the rims indicate an increase in pressure and decrease in temperature during garnet growth. Garnet rim compositions are consistent with modelled isopleths in the phase fields with the assemblages including Grt-Bt-Pl-Ilm-Cc-Qtz±Amph±Cpx. In addition to the garnet isopleths, matrix plagioclase compositions (X_{An}) were also used to constrain the P-T estimate to 650-670 °C and 10.8 – 12.3 kbar (Fig. 10B). Modelled X_{Mg} values for biotite also agree well with measured values. The estimate is also consistent with the presence of calcite as inclusions in garnet rims and as a phase in the matrix (Fig. 7B). Modelled modal% predicts up to 14 modal% calcite, which is consistent with observations in the sample.

Microstructures showing amphibole, quartz and calcite together, and calcite replacing plagioclase suggest the following reaction occurred during the higher-pressure metamorphism: Cpx + Pl + CO_2 + H_2O = Hbl + Cc + Qtz. The S-shaped inclusion trails in some garnet grains (including calcite), indicate some syn-tectonic garnet growth. Modelled garnet modal% indicates an increase from 8 modal% for the conditions of the core estimate to ~18 modal% for the conditions of the rim estimate, which is consistent with observed garnet content, and consistent with garnet growth with the increase in pressure between core and rim estimates. The garnet compositions and conditions for metamorphism suggest that the rock records initial higher-temperature amphibolite facies conditions followed by slightly lower-temperature, higher-pressure amphibolite-facies conditions associated with the influx of a CO_2-H_2O fluid. Thin rims on garnet that show a decrease in X_{Mg} content and increase in Sps content likely reflect later retrogression during decreasing pressure and temperature. It should be noted that the estimate for conditions during garnet core formation is an apparent estimate as garnet cores may have been modified by later diffusion, and because the bulk composition used for the calculation better represents the later metamorphic overprint.

7.3 Lower Skjervøy (S8d)

The presence of an early foliation (pre-S2?) displayed by garnet inclusions that also display a different mineral paragenesis to the matrix shows that the rock records evolving P-T conditions. Measured garnet core compositions match modelled values with Grt-Bt-Chl-Ms-Pg-Ilm-Qtz stable at 540 - 560 °C and 8.5 – 10.3 kbar (Fig. 11A), consistent with chlorite and ilmenite inclusions in garnet (Fig. 7D). Modelled isopleths match measured garnet rim compositions in the phase field Grt-Bt-Pl-Ms-Rt-Qtz at 645 – 665 °C and 12.3 – 13.8 kbar (Fig. 11A), consistent with the matrix S2 assemblage. Modelled values for X_{Mg} in biotite and Si content in white mica match this estimate well. Modelled values for anorthite content in plagioclase plot at slightly lower pressures (~1 kbar) than the rim estimate. The shape of the garnet profile for X_{Mg}, Grs and Alm (Fig, 8B) suggests that zoning in garnet is a result of growth zoning. In addition, garnet modal% increases with increasing pressure and temperature between the garnet core and rim estimates, which is consistent with prograde garnet growth.

7.4 Upper Skjervøy (S174a)

The matrix of sample S174a preserves an S2 foliation, however the shape of the garnet profile suggests garnet may record a multi-stage history, and the presence of inclusions in garnet that are not stable in the matrix suggests the rock records evolving P-T conditions (Figs. 7F, 8C). Garnet core compositions correspond with modelled isopleths in the phase field Grt-Bt-Ilm-Hd-Ath-Act-Qtz at 620 – 640 °C and 4.7 – 5.6 kbar (Figs. 11B, C). Composition of mid-garnet matches modelled compositions in the Grt-Bt-Chl-Pl-Ilm-Zo-Qtz phase field at 490 – 520 °C and 7.2 – 8.3 kbar (Figs. 11B, C), which is consistent with the presence of chlorite and ilmenite inclusions in mid-garnet. Garnet rim compositions match modelled values with Grt-Bt-Pl-Ms-Ttn-Qtz stable at 580-630 °C and 11.4 – 14 kbar (Figs. 11B, C), and is consistent with the presence of muscovite and titanite in the matrix. In addition, measured X_{Mg} values for biotite and anorthite content in plagioclase in the matrix match modelled values that give a range between the mid-garnet and garnet core estimate. Si content in muscovite matches modelled values that fit with the rim estimate. The shape of modelled garnet modal% isopleths show that garnet growth is possible following a path between the three estimates and the morphology of the

compositional isopleths along the P-T path (black arrows; Figs. 11B, C) also reproduces the garnet profile well (Fig. 8C).

7.5 Kågen (S17)

Sample S17 preserves the S2 foliation, however the presence of both staurolite and kyanite together indicates the sample records evolving P-T conditions. Since fine-grained kyanite overgrows staurolite, kyanite represents part of the peak S2 paragenesis. The presence of kyanite, and lack of biotite and plagioclase constrains metamorphism above ~10 kbar and below ~700 °C (Fig. 11D). A complete lack of zoning in garnet, despite its microstructure, suggests that garnet compositions have been reset by diffusion during peak metamorphism (Fig. 9A). Measured garnet compositions fit modelled isopleths in the Ms-Grt-Ky-Pg-Qtz-Rt phase field at 670 – 705 °C and 10 – 11.1 kbar (Fig. 11D), which is mostly consistent with the matrix assemblage. Si content in muscovite is consistent with the estimate. Paragonite was not observed, but is predicted as less than 1 modal% of the assemblage and therefore could be present. Kyanite and garnet probably grew together, consuming quartz and staurolite by the reaction St + Qtz = Grt + Ky + H_2O during prograde metamorphism.

7.6 Uløya (UL250)

Microstructures in sample UL250 indicate that garnet grew during S2 shearing. Slight zoning in spessartine and X_{Mg} in some garnets indicates growth during prograde metamorphism, although the majority of cores and rim compositions show little variation and probably indicate equilibration at peak conditions. Garnet compositions match modelled compositions in the phase field Grt-Bt-Pl-Rt-Qtz at 610 – 650 °C and 10 – 11.3 kbar (Fig. 12A). Measured values for X_{Mg} in biotite and anorthite content in plagioclase match modelled isopleths over a range that includes the estimate and down to lower P-T. Although garnet core compositions do not record earlier P-T conditions, the presence of chlorite inclusions suggest that the initial garnet growth was in the chlorite stability zone and that metamorphism followed a prograde path (black arrow; Fig. 12A). Si content in muscovite fits modelled compositions either at lower P-T or higher P than the estimate. Since biotite mostly overgrows muscovite in the sample, it is more likely that the majority

of the muscovite grew early at a lower P-T during prograde metamorphism along with minor zoisite and abundant titanite in the matrix.

7.7 Vaddas-Kalak boundary (AR186)

Only minor zoning in garnet, and a relative lack of compositional variation in matrix minerals, suggests the S2 foliation in sample AR186 best represents an equilibrium paragenesis relative to the other samples. It is also the most strongly deformed sample. The relative increase in grossular and spessartine content, and decrease in X_{Mg} between cores and rims indicates a slight increase in pressure between garnet core and rim compositions (Table 3; Figs. 9C, 12B). Measured garnet compositions correspond with modelled isopleths in the phase fields Grt+Pl+Bt+Pl+Kfs+Ms+Qtz±Rt±Ttn at 680 - 705 °C and 13.5 - 15 kbar (Fig. 12B). Garnet cores generally correspond with the rutile-bearing phase field, whereas rims plot entirely in the lower temperature titanite-bearing field, which is consistent with titanite as the dominant Ti-bearing phase in the matrix. Measured X_{Mg} in bioitite, An in plagioclase and Si content in white mica corresponds well with modelled values for the estimated P-T range, and biotite and plagioclase compositions agree with the upper pressure limit defined by the garnet composition. Although garnet core compositions do not indicate significantly lower temperature conditions, the presence of chlorite inclusions suggests garnet initially grew at lower P-T and that its current composition is a result of later diffusion.

8. Metamorphism in the KNC in the study area

All the phase equilibrium models presented use the same thermodynamic datasets and, with the exception of samples ST257 and ST254b, the same solid-solution models, so that systematic and random errors related to these affect the P-T estimates similarly. Care was taken to ensure that analytical techniques recorded comparable data, and that XRF bulk analysis sample size best represented the equilibration volume. Therefore relative differences between P-T estimates are likely real. Bulk composition is the primary control on pseudosection topology, and it should be noted that geological errors related to bulk composition variation (e.g. lack of chemical homogeneity in the sample volume, temporal bulk composition change related to lack of communication of mineral cores with the

matrix, and melt/fluid presence) can introduce errors in P-T estimates of ± 50 °C and 0.5 kbar, and up to 1 kbar in some cases (e.g. Palin et al., 2016).

Several samples display pre-S2 metamorphic conditions. In the lower part of the KNC in Straumfjord the $S1^S$ foliation records epidote-amphibolite to lower amphibolite facies metamorphism (Fig. 10A, 13A; 530 – 570 °C and 8.2 – 9.3 kbar). Garnet cores in sample S8d, from the lower rocks of the KNC on Skjervøy, record apparent conditions at similar lower amphibolite facies conditions (Fig. 11A, 13A; 540 - 560 °C and 8.5 – 10.3 kbar), suggesting both units, at similar tectonostratigraphic levels, record the same pre-Caledonian lower amphibolite facies event. The pre-S2 apparent conditions recorded by garnet cores from rocks at the top of the lower meta-arkose unit on Skjervøy (sample S174a) show an early high-temperature, low-pressure event (620-640 °C and 4.7-5.6 kbar; Figs. 11, B, C, 13A), not recorded by any other samples. This early high-temperature metamorphism was followed by cooling to lower temperature, slightly higher-pressure conditions at 490-520 °C and 7.2-8.3 kbar and then higher pressure and temperature S2 shearing (Fig. 13A). We therefore interpret that the high temperature event is pre-Caledonian as it was followed by a period of cooling prior to prograde metamorphism related to Caledonian shearing.

P-T conditions for the S2 foliation in all the KNC samples record Caledonian metamorphism (Fig. 13A). In Straumfjord S2 syn-kinematic garnet growth (ST257) records a possible two-phase Caledonian evolution with: 1) apparent early high-temperature, low-pressure conditions (675 – 690 °C and 8.3- 9 kbar; Fig. 10B, 13A), followed by 2) higher pressure, lower temperature conditions recorded by an increase in grossular and X_{Mg} contents towards garnet rims (650-670 °C and 10.8 – 12.3; Figs. 10B, 13A). The higher pressure conditions are more similar to typical S2 metamorphism in other samples (Fig. 13A, B, C). With the exception of the lower greenschist facies units, the peak S2 conditions (peak pressure) indicate high-pressure amphibolite facies metamorphic conditions throughout most of the KNC in the field area (580 – 710 °C and 10 -14 kbar). Although the range in temperature across the units is not large, and estimates are all within error of one another (considering a standard error of ± 50 °C; Fig.

13B), the relative differences show some interesting trends. Within both the upper and lower nappes, the highest temperatures are recorded in the nappe cores furthest from the major boundaries (650-660 °C in the core of the lower nappe and 660-700 °C in the core of the upper nappe; Fig. 13A, B), while the lowest temperatures are recorded at the boundary between the upper and lower KNC (575 – 650 °C: Figs. 13A, B). Still lower temperatures occur in the lowermost KNC rocks (< 490 °C: Rice, 1987). The highest temperature is displayed by the rocks from the KNC-RNC boundary (~700 °C; Figs. 13A, B). The variation in S2 peak pressure is more significant than the temperature variation (Figs 13A, C). In the lower nappe the pressure increases upwards to the boundary between the upper and lower KNC. The pressure in the upper KNC is slightly lower than the lower KNC, and pressure in the nappe stack is highest along the RNC-KNC boundary (13.8 - 15 kbar; Figs. 13A, C). This estimate has a slightly higher pressure than a previous estimate for metamorphism along this boundary, even considering an uncertainty of ± 1 kbar (12-13 kbar; Faber et al., in prep.). In general, shearing along the major nappe boundaries recognized in the area display decreasing P-T downwards in the tectonostratigraphy, with low eclogite facies conditions along KNC-RNC boundary, amphibolite facies conditions along the boundary between the upper and lower KNC, and greenschist facies conditions in the lower units of the KNC.

9. Discussion of the metamorphic evolution of the KNC

Pre-S2 fabrics and metamorphic relicts in the KNC, overprinted by Caledonian metamorphism (S2), record individual parts of a long-lived history. Rice (1984, 1985, 1987) first documented the increase in temperature upwards in the KNC, and recognized the preservation of an S1 foliation within garnet. He interpreted the S1 as part of early stage burial in the Caledonian cycle. However, we now know that the KNC has undergone a polyphase metamorphic history, spanning the entire Neoproterozoic (e.g. Daly et al., 1991; Kirkland et al., 2005, 2006a, 2007b; Corfu et al., 2007, 2011; Gasser et al., 2015). The difference in metamorphic conditions in pre-S2 relicts for samples taken in different nappes suggest that the nappes record different parts of a pre-Caledonian evolution. Specifically, the pressure variations between pre-Caledonian and Caledonian events indicate that they occurred at different levels in the crust, and contrasting

geothermal gradients for the events suggest they record different tectonic settings (Table 4; Fig. 13A, 14). In addition, variations in Caledonian metamorphic conditions within the nappes of the KNC shed light on the evolution of the nappes during continental collision and nappe stacking.

9.1 Pre-Caledonian evolution

9.1.1 Lower KNC

Pre-Caledonian metamorphic conditions in the lower nappes in Straumfjord and on Skjervøy indicate that the lower part of the KNC underwent the same event (~550°C, 8-10 kbar; Figs. 10A, 11A, 13A, 14). These sets of conditions indicate a geothermal gradient typical of regional metamorphism (~18-20 °C/km). Since the $S1^S$ foliation is folded on northern Skjervøy, and subsequently crosscut by pegmatitic granites and fine-grained mafic dykes, we interpret that the estimated conditions probably record metamorphism during an orogenic event prior to at least two different phases of pre-Caledonian intrusion. These rocks show similarities to the lower KNC in Finnmark, where the nappes include Paleoproterozoic orthogneiss of the Fagervik Complex and overlying metapsammites and schists of the 1030 – 980 Ma Sværholt succession. There the rocks were deformed at similar metamorphic conditions (biotite-grade) prior to the intrusion of Grenvillian/Sveconorwegian (~980 Ma) granites, and appear to record little subsequent deformation or metamorphism prior to the Caledonian orogeny (Kirkland et al., 2006a, 2007a, 2008b; Corfu et al., 2011). The style of pre-Caledonian folding in the lower KNC in the field area matches that described in Finnmark (e.g. Ramsay et al., 1985; Kirkland et al., 2006a, 2006b). Based on the tectonostratigraphic position of the rocks, fold styles, and crosscutting relationships, we suggest that the lower nappe in the field area is equivalent to the lower nappes described in Finnmark (including the Fagervik Complex and Sværholt succession) and that regional metamorphism associated with the $S1^S$ foliation may be equivalent to the early biotite-grade foliation attributed to the Grenvillian/Sveconorwegian in Finnmark (Fig. 14).

Apparent pre-Caledonian high-temperature metamorphic conditions indicated by garnet cores in the lower meta-arkose on Skjervøy (620 – 640 °C and 4.7 – 5.6 kbar; Table 4;

Figs. 11B, 13A, 14) are not seen in the rest of the rocks in the lower KNC. This event suggests an elevated geothermal gradient (~40 °C/km) for this pre-Caledonian metamorphism. Given the tectonostratigraphic position of the sample at the boundary between the lower meta-arkose and the upper KNC nappe, the rocks may record conditions related to juxtaposition of the upper and lower nappes. Kirkland et al., (2005) noted ~700 Ma overgrowths on zircon in lower KNC rocks and speculated that they recorded the juxtaposition of the upper and lower KNC at that time. The high-temperature event in the lower meta-arkose at the boundary between the upper and lower parts of the KNC may therefore be related to the high-temperature metamorphism recorded in the upper nappe at ~700 Ma, within a shallower part of the crust (e.g. Gasser et al., 2015. Fig. 14). The upper nappe also records high-temperature conditions related to intrusives in the Corrovarre nappe (at 610 Ma and 5.5-6.5 kbar; Zwaan and van Roermund, 1990; Gee et al., 2017) and the Seiland Igneous Province (at 520-580 Ma and 5-7 kbar; Elvevold et al., 1994; Roberts et al., 2006). Therefore, it is also possible that the pre-Caledonian low-pressure, high-temperature conditions at the boundary record local elevated temperatures imposed by either of these intrusive events, based on the similarity of the estimated pressures for the events. However, the events related to the SIP and Corrovarre intrusions have not been previously described in the lower KNC nappes.

9.1.2 Upper KNC

Based on detrital zircons, the paragneisses of the upper KNC correlate with the Sørøy succession in the upper nappes in Finnmark, deposited between 920-840 Ma (Fig. 14; Kirkland et al., 2006a, 2016; Corfu et al., 2007; Gasser et al., 2015). Structures in the paragneisses show widespread evidence for pre-Caledonian granulite-facies migmatisation, similar to that described by Gasser et al., (2015), and we therefore interpret that their S1 foliation is the $S1^{E}$ foliation described in this work. We show that this event is widespread in the upper nappe and not preserved only locally. The conditions of this event were constrained above the solidus at 760 – 775 °C and 8.8-9.8 kbar and ~700 Ma (Corfu et al., 2007; Gasser et al., 2015; Table 4; Fig. 13A, 14). The metamorphic conditions of the $S1^{E}$ event reflect a relatively normal continental geotherm (~25 °C/km), suggesting high-grade regional metamorphism. Although the upper meta-

arkose unit does contain sheared felsic lenses, the sample used for phase equilibrium modelling showed no evidence for an early high-grade metamorphic event (UL250; Fig. 13A), and its relationship with the underlying paragneiss is therefore less clear. The lack of preservation of an earlier event is likely due to strong S2 re-equilibration of pre-existing mineral parageneses.

9.2 Caledonian evolution

The S2 foliation, with its associated stretching lineation and top-to-SE or top-to-E shear sense indicators records Caledonian nappe emplacement (Ramsay et al., 1985). The upper amphibolite-facies conditions estimated for Caledonian metamorphism in the KNC indicate mid- to lower-crustal metamorphism with a relatively low geothermal gradient (14-20 °C/km), reflecting crustal thickening. The pressure increase with respect to pre-Caledonian conditions probably indicates the onset of subduction of continental crust (KNC) during continental collision. The age of Caledonian metamorphism is dated in the upper part of the KNC at Eide by titanite growth associated with the S2 shearing between 440 – 430 Ma (Gasser et al., 2015; Fig. 14). Metamorphic garnet and metasomatic zircon growth in the lower nappes in Finnmark date metamorphism at 436 ± 21 Ma and 428 ± 4 Ma, respectively (Kirkland et al., 2007a), indicating that amphibolite-facies metamorphism in the upper and lower parts of the KNC may have occurred together over the same protracted 10 Ma-long time period (Fig. 14).

The two phases of Caledonian metamorphism (both at high T, the later at high P) recorded in the rocks at Straumfjord are consistent with observations of two phases of muscovite grown at different metamorphic conditions that indicate different Silurian ages in lower KNC rocks in Finnmark (Kirkland et al., 2007a). The higher phengite content and lower Ti content of the younger muscovite relative to the older one indicates that early muscovite grew at lower pressures and higher temperatures relative to the younger one. Early muscovite recorded an $^{40}Ar/^{39}Ar$ cooling age of 439 ± 3 Ma, while later muscovite gave an $^{40}Ar/^{39}Ar$ cooling age of 420 ± 3 Ma (Kirkland et al., 2007a). While these are cooling ages, and cannot be directly related to the peak P-T conditions determined in this work, they nevertheless show a two-phase anticlockwise Caledonian

history in the KNC with high temperature, low pressure conditions prior to ~440 Ma, and higher pressure, lower temperature conditions prior to 420 Ma. This counterclockwise P-T evolution during the early Caledonian suggests that initial metamorphism and deformation had some additional heat input at least ~10 Ma prior to burial to peak pressures (Fig. 14). Since garnet in sample ST257 that records both P-T conditions grew syn-kinematically with the S2 foliation, both events are related to compression during the Caledonian orogeny. The counterclockwise P-T path recorded for Caledonian metamorphism here is also observed in the overlying RNC. Anticlockwise P-T paths most often occur in rocks that experience early granulite facies metamorphism in an extensional setting, followed by contraction (e.g. continental collision and crustal thickening; Wakabayashi, 2004). A common explanation for such a situation is subduction of a back-arc (e.g. Johnson and Strachan, 2006). However, this interpretation for northern Norway is problematic (e.g. Faber et al., in prep.).

10. Implications for assembly of the KNC

10.1 Pre-Caledonian assembly

The origin of the KNC and timing and context of its assembly are controversial (e.g. Kirkland et al., 2006a, 2007b: Corfu et al., 2007, 2011; Gee et al., 2017). There is an ongoing debate between two main arguments: 1) the KNC formed at the Baltica margin, and preserves Timanian elements not seen elsewhere in the Caledonides (e.g. Zhang et al., 2016; Gee et al., 2017), or 2) the KNC was initially amalgamated elsewhere (potentially at the Laurentia margin) and subsequently accreted to Baltica, probably by strike-slip movement during overall oblique convergence during the Caledonian orogeny (e.g. Kirkland et al., 2006a, 2007b; Corfu et al., 2007, 2011). The lack of typical oceanic rocks between the KNC and the Baltica basement, or within the KNC, is in opposition with models that describe the KNC as a far-travelled exotic terrane.

The lower KNC nappe contains Baltican elements (the Fagervik Complex). It also probably records Sveconorwegian events in the metasediments of the nappe, which although not represented in the current Baltican basement in northern Norway, does not preclude its origin on the palaeo-Baltica margin (e.g. Gee et al., 2017). In addition, it is

not clear whether low-grade metamorphism in the eastern-most units of the KNC represents mostly Caledonian or pre-Caledonian events (e.g. Kirkland et al., 2008a). Migmatisation at ~700 Ma in the upper nappes is not widely recorded in the lower nappe, and they must therefore have been juxtaposed during or after ~700 Ma. The local ~700 Ma overgrowths on zircon recognized in the lower nappe in Finnmark (e.g. Kirkland et al., 2005), and the possible record of ~700 Ma metamorphism at the boundary between the upper and lower KNC allows us to speculate that the juxtaposition of the upper KNC with the rocks below occurred at this time. If the pre-Caledonian high-temperature metamorphism instead records heating from intrusions in the Corrovarre nappe or the SIP, then it would indicate that the lower KNC was affected by these events, and that the rocks were probably juxtaposed together (at the palaeo-Baltica margin) before ~600 Ma. In either scenario, the upper and lower KNC were juxtaposed together prior to the Caledonian Orogeny.

10.2 Nappe stacking during the Caledonian orogeny

The nappes in the KNC preserve pervasive S2 deformation representing the development of lower crustal nappes. The age range preserved in the amphibolite facies rocks of the KNC and RNC indicate that this stage in the continental collision occurred in both nappes at around the same time, between 440 – 430 Ma (Gasser et al., 2015; Faber et al., in prep.). Greenschist facies metamorphism in the lowermost KNC is recorded between 425-420 Ma (Kirkland et al., 2008a), representing final emplacement of the KNC nappe stack at higher crustal levels. The metamorphic estimates for S2 shearing presented in this paper records the history of ductile nappe stacking in the lower crust during crustal thickening at 35 – 50 km depth. Such deformation facilitates large-scale mid- to lower crustal ductile flow. The relative differences in metamorphic conditions within the nappes show that conditions do not increase linearly and continuously upwards in in the nappe stack, and indicate that although deformation was pervasive, the rocks do comprise several individual nappes that record slightly different conditions in their cores. The relative increase in P-T upwards with respect to major nappe boundaries indicates that the inverted metamorphic gradient is a result of progressive nappe stacking towards increasingly higher levels in the crust. Local differences in P-T within nappes are likely

due to temporal variation, with nappe cores recording slightly earlier deformation and metamorphism and nappe boundaries equilibrating slightly later during nappe stacking. The higher pressures in the lower KNC nappe with respect to the upper nappe may reflect underthrusting of the upper nappe by the lower nappe during Caledonian crustal thickening.

The change from low-greenschist facies in the lowermost units of the KNC to upper amphibolite facies in the upper units is further evidence that the KNC is comprised of several nappes of different metamorphic grade. Since the gradient from greenschist facies up to amphibolite facies is most pronounced in the lower units it is likely that the lower thrust nappes accommodated most of the latest deformation and final nappe emplacement, with little continued deformation in the upper part of the KNC. Final emplacement of the KNC occurred at greenschist facies, recorded only in the lowermost units (e.g. at Rotsundelv and Sorkjøsen; Fig. 2), and is dated in Finnmark at ~425 Ma (Kirkland et al., 2008a). These conditions record the last local movements of the KNC.

11. Implications for continental collision in the northern Caledonides

The establishment of structural heterogeneities and modification of water content and mineral paragenesis during metamorphism imposed by pre-Caledonian events probably had an impact on re-working of the crustal rocks during Caledonian continental collision. The difference in pre-Caledonian metamorphic grade of the upper and lower nappes (that led to different metamorphic mineral assemblages), development of different structures, and the difference in overall bulk composition (quartz-feldspar orthogneiss and meta-arkose in the lower nappe vs. metasediments and amphibolites in the upper nappe) likely had an impact on the subsequent behaviour of the rocks during the formation of crustal nappes. The difference in rheology may have facilitated underthrusting of the upper nappe by the lower nappe during continental collision due to differences in overall strength, where the lower nappe rocks were stronger and more rigid (orthogneiss and meta-arkose) than the upper nappe rocks (foliated paragneisses). In addition, the early Caledonian heating event, preserved in sample ST257 probably enhanced ductility of the rocks, promoting pervasive ductile deformation.

12. Conclusions

The field data and tectonostratigraphic descriptions show that the western part of the KNC, exposed in the study area, consists of three main nappes; 1) a lowermost greenschist facies nappe, 2) a lower nappe probably correlative of the lower nappes in Finnmark, including the Fagervik Complex and Sværholt succession, which preserves relicts of a pre-Caledonian $S1^S$ foliation, and 3) an upper nappe comprised of polymetamorphic paragneisses that is correlative of the Sørøy succession in Finnmark, which preserves a pre-Caledonian $S1^E$ foliation. The $S1^E$ foliation has been previously studied and records migmatisation at granulite facies conditions at ~700 Ma (Gasser et al., 2015). The $S1^S$ foliation records epidote-amphibolite facies to lower amphibolite facies metamorphism, which may be related to Grenvillian/Sveconorwegian deformation and regional metamorphism. Rocks from the boundary between the upper and lower KNC record pre-Caledonian high temperature, low pressure metamorphism related to either: 1) juxtaposition of the upper and lower KNC at ~700 Ma, or 2) local elevated temperatures caused by the intrusion of the Corrovarre dyke swarm at ~610 Ma or the Seiland Igneous Province at ~580-520 Ma. An early high-temperature, low-pressure phase in the Caledonian overprint may indicate that the KNC rocks underwent the same Caledonian anticlockwise P-T path recorded in the overlying RNC. The Caledonian metamorphic overprint (S2) reflects high-pressure amphibolite to low eclogite facies conditions, indicating burial to lower-crustal conditions and nappe stacking during crustal thickening at the onset of continental collision. Major nappe boundaries display a relative increase in P-T upwards, displaying an inverted metamorphic gradient consistent with in-sequence nappe stacking. Variations in P-T within the nappes is likely temporal, and higher pressures in the lower KNC relative to the upper KNC nappe probably records underthrusting of the upper nappe by the lower nappe during crustal thickening.

References

Akselsen, J., 1982. Precambrian and Caledonian tectonometamorphic evolution of northeaster Seiland, Finnmark, north Norway, Norges Geologiske Undersøkelse, 373, 45-61.

Andresen, A., 1988. Caledonian terranes of northern Norway and their characteristics. Trabajos de Geologia, University of Oviedo, 17, 103-117.

Augland, L.E., Andresen, A., Gasser, D., and Steltenpohl, M.G., 2014. Early Ordovician to Silurian evolution of exotic terranes in the Scandinavian Caledonides of the Ofoten-Troms area – terrrane characterization and correlation based on new U.Pb zircon ages and Lu-Hf isotopic data, Geological Society, Longon, Special Publications, 390, 655-678.

Andréasson, P.G., Gee, D.G., Whitehouse, M.J., and Schöberg, H., 2003. Subduction-flip during Iapetus Ocean closure and Baltica-Laurentia collision, Scandinavian Caledonides, Terra Nova, 15, 362-369.

Austrheim, H., 1991. Eclogite formation and dynamics of crustal roots under continental collision zones, Terra Nova, 3, 492-499.

Coggon, R. & Holland, T.J.B., 2002. Mixing properties of phengitic micas and revised garnet-phengite thermobarometers. Journal of Metamorphic Geology, 20, 683-696.

Connolly, J.A.D., 2005. Computation of phase equilibria by linear programming: a tool for geodynamic modelling and its application to subduction zone decarbonation. Earth and Planetary Science Letters, 236, 524–541.

Corfu, F., Roberts, R.J., Torsvik, T.H., Ashwal, L.D., Ramsay, D.M., 2007. Peri-Gondwanan elements in the Caledonian nappes of Finnmark, northern Norway: implications for the paleogeographic framework of the Scandianvian Caledonides, 307, 434-458.

Corfu, F., Gerber, M., Andersen, T.B., Torsvik, T.H., and Ashwal, L.D., 2011. Age and significance of Grenvillian and Silurian orogenic events in the Finnmarkian Caledonides, northern Norway, Canadian Journal of Earth Sciences, 48, 419-440.

Dallmeyer, R.D., 1988. Polyorogenic $^{40}Ar/^{39}Ar$ mineral age record within the Kalak Nappe Complex, Northern Scandinavian Caledonides, Journal of the Geological Society, 145. 705-716.

Daly, J.S., Aitcheson, S.J., Cliff, R.A., Gayer, R.A., and Rice, A.H.N., 1991. Geochronological evidence from discordant plutons for a late Proterozoic orogeny in the Caledonides of Finnmark, northern Norway, Journal of the Geological Society, London, 148, 29-40.

Elvevold, S., and Andersen, T., 1993. Fluid evolution during metamorphism at increasing pressure: carbonic- and nitrogen-bearing fluid inclusions in granulites from Øksfjord, north Norwegian Caledonides, Contributions to Mineralogy and Petrology, 114, 236-246.

Elvevold, S., Reginiussen, H., Krogh, E.J., and Bjørklund, F., 1994. Reworking of deep-seated gabbros and associated contact metamorphosed paragneisses in the southeastern part of the Seiland Igneous Province, northern Norway, Journal of Metamorphic Geology, 12, 539–556.

Escher, A., Masson, H., and Steck, A., 1993. Nappe geometry in the western Swiss Alps, Journal of Structural Geology, 15, 501-509.

Escher, A., and Beaumont, C., 1997. Formation, burial and exhumation of basement nappes at crustal scale: a geometric model based on the Western Swiss-Italian Alps, Journal of Structural Geology, 19, 955-974.

Fuhrman, M.L. & Lindsley, H., 1988. Ternary-feldspar modelling and thermometry. American Mineralogist, 73, 201–215.

Gasser, D., Jerabek, P., Faber, C. Stünitz, H., Menegon, L., Corfu, F., Erambert, M., and Whitehouse, M.J., 2013. Behaviour of geochronometers and timing of the metamorphic reactions during deformation at lower crustal conditions: phase equilibrium modelling and U-Pb dating of zircon, monazite, rutile and titanite from the Kalak Nappe Complex, northern Norway, Journal of Metamorphic Geology, 33, 513-534.

Gayer, R. A., Humphreys, U. J., Binns, R. E., and Chapman, T., 1985. Tectonic modelling of the Fiimmark and Troms Caledonides based on high level igneous rock geochtmistry, in Gee, D. G., and Sum, B. A., eds.. The Caledonide orogen — Scandinavia and related areas: Chichester, England, Wiley & Sons, 931-951.

Gayer, R.A., Rice, A.H.N., Roberts, D., and Townsend, C., 1987. Restoration of the Caledonian Baltoscandian margin from balanced cross-sections: the problem of excess continental crust, Earth and Environmental Science Transactions of The Royal Society of Edinburgh, 78, 197-217.

Gee, D.G., Andréasson, P.G., Li, Y., and Krill, A., 2017. Baltoscandian margin, Sveconorwegian crust, lost by subduction during Caledonian collisional orogeny, GFF: Journal of the Geological Society of Sweden, 139, 36-51.

Holland, T.J.B., Powell, R., 1996. Thermodynamics of order-disorder in minerals. 2. Symmetric formalism applied to solid solutions. American Mineralogist 81, 1425-1437.

Holland, T.J.B., Powell, R., 1998. An internally consistent thermodynamic data set for phases of petrological interest. Journal of Metamorphic Geology 16, 309-343.

Holland, T., and Powell, R., 2003. Activity-composition relations for phases in petrological calculations: an asymmetric multicomponent formulation, Contributions to Mineralogy and Petrology, 145, 492-501.

Johnson, M.R.W., and Strachan, R.A., 2006. A discussion of possible heat sources during nappe stacking: the origin of Barrovian metamorphism within the Caledonian thrust sheets of NW Scotland, Journal of the Geological Society, London, 163, 579-582.

Kirkland, C.L., Daly, J.S., and Whitehouse, M., 2005. Granitic magmatism of Grenvillian and late Neoproterozoic age in Finnmark: constraining pre Scandian deformation in the Kalak Nappe Complex. Precambrian Research, 145, 24-52.

Kirkland, C.L., Daly, J.S., and Whitehouse, M.J., 2006a. Granitic magmatism of Grenvillian and late Neoproterozoic age in Finnmark, Arctic Norway – constraining pre-Scandian deformation in the Kalak Nappe Complex, Precambrian Research, 145, 24-52.

Kirkland, C.L., Daly, J.S., Eide, E.A., and Whitehouse, M.J., 2006b. The structure and timing of lateral escape during the Scandian Orogeny: A combined strain and geochronological investigation in Finnmark, Arctic Norwegian Caledonides, Tectonophysics, 425, 159-189.

Kirkland, C.L., Daly, J.S., Eide, E.A., and Whitehouse, M.J., 2007a. Tectonic evolution of the arctic Norwegian Caledonides from a texturally- and structurally- constrained multi-isotopic (Ar-Ar. Rb-Sr, Sm-Nd, U-Pb) study, American Journal of Science, 307, 459-526.

Kirkland, C.L., Daly, J.S., and Whitehouse, M.J., 2007b. Provenance and terrane evolution of the Kalak Nappe Complex, Norwegian Caledonides: implications for Neoproterozoic paleogeography and tectonics, The Journal of Geology, 115, 21-41.

Kirkland, C.L., Daly, J.S., Chew, D.M., and Page, L.M., 2008a. The Finnmarkian orogeny revisited: an isotopic investigation of eastern Finnmark, Arctic Norway, Tectonophysics, 460, 158-177.

Kirkland, C.L., Daly, J.S., and Whitehouse, M.J., 2008b. Basement-cover relationships of the Kalak Nappe Complex, Arctic Norwegian Caledonides and constraints on Neoproterozoic terrane assembly in the North Atlantic region, Precambrian Research, 160, 245-276.

Kirkland, C.L., Erickson, T.M., Johnson, T.E., Danisik, M., Evans, N.J., Bourdet, J., and McDonald, B.J., 2016. Discriminating prolonged, episodic or disturbed monazite age spectra: An example from the Kalak Nappe Complex, Arctic Norway, Chemical Geology, 424, 96-110.

Kvassnes, A.J.S., Strand, A.H., Moen-Eikeland, H., and Pedersen, R.B., 2004. The Lyngen Gabbro: the lower crust of an Ordovician Incipient arc, Contributions to Mineralogy and Petrology, 148, 358-379.

Lindahl, I., Stevens, B.P.J., and Zwaan, K.B., 2005. The geology of the Vaddas area, Troms: a key to our understanding of the Upper Allochton in the Caledonides of northern Norway, NGU Bulletin, 445, 5-43.

Menegon, L., Nasipuri, P., Stünitz, H., Behrens, H., and Ravna, E., 2011. Dry and strong quartz during deformation of the lower crust in the presence of melt, Journal of Geophysical Research Solid Earth, 116, B10410.

Palin, R.M., Weller, O.M., Waters, D.J., and Dyck, B., 2016. Quantifying geological uncertainty in metamorphic phase equilibria modelling; a Monte Carlo assessment and implications for tectonic interpretations, Geoscience Frontiers, 7, 591-607.

Ramsay, D.M., Sturt, B.A., Zwaan, K.B., and Roberts, D., 1985. Caledonides of Northern Norway, in Gee, D.G., and Sturt, B.A. (eds), The Caledonian Orogen – Scandinavia and Related areas: New York, Wiley, 163-184.

Rice, A.H.N., 1984. Metamorphic and structural diachroneity in the Finnmarkian nappes of northern Norway, Journal of Metamorphic Geology, 2, 219-236.

Rice, A.H.N., 1985. Staurolite growth and metamorphic zones in the Kalak Nappe Complex of northeastern Porsangerhalvøya, north Norway, Lithos, 18, 281-294.

Rice, A.H.N., 1987. Continuous out-of-sequence ductile thrusting in the Norwegian Caledonides, Geological Magazine, 124, 249-260.

Rice, A.H.N., and Frank, W., 2003. The early Caledonian (Finnmarkian) event reassessed in Finnmark $^{40}Ar/^{39}Ar$ cleavage age data from NW Varangerhalvøya, N. Norway, Tectonophysics, 374, 219-236.

Roberts, D., 1973. Geologisk kart over Norge, berggrunnskart,. Hammerfest 1:250 000, Norges Geologiske Undersøkelse.

Roberts, D., and Sturt, B.A., 1980. Caledonian deformation in Norway, Journal of the Geological Society, 137, 241-250.

Roberts, D., 1985. The Caledonian fold belt in Finnmark: a synopsis. Norges Geologiske Undersøkelse, 403, 161–177.

Roberts, D., 1990. Geochemistry of mafic dykes in the Corrovarre Nappe, Troms, North Norway, NGU-Bulletin, 419, 45-53.

Roberts, D., 2003. The Scandinavian Caledonides: event chronology , paleogeographic settings and likely modern analogues, Tectonophysics, 365, 283-299.

Roberts, R.J., Corfu, F., Torsvik, T.H., Ashwal, L.D. & Ramsay, D.M., 2006. Short-lived mafic magmatism at 560- 570 Ma in the northern Norwegian Caledonides: U-Pb zircon ages from the Seiland Igneous Province. Geological Magazine, 143, 887 903.

Roberts, R.J., Corfu, F., Torsvik, T.H., Hetherington, C.J. & Ashwal, L.D., 2010. Age of alkaline rocks in the Seiland Igneous Province, Northern Norway. Journal of the Geological Society of London, 167, 71–81.

Rosenberg, C.L., and Handy, M.R., 2005. Experimental deformation of partially melted granite revisited: implications for the continental crust, Journal of Metamorphic Geology, 23, 19-28.

Schmid, S.M., Fügenschuh, B., Kissling, E., and Schuster, R., 2004. Tectonic map and overall architecture of the Alpine orogen, Eclogae Geologicae Helvetiae, 97, 93-117.

Slagstad, T., Melezhik, V.A., Kirkland, C.L. et al., 2006. Carbonate isotope chemostratigraphy suggests revisions to the geological history of the West Finnmark Caledonides, northern Norway. Journal of the Geological Society of London, 163, 277–289.

Stephens, M.B., and Gee, D.G., 1985. A tectonic model for the evolution of the eugeoclinal terranes in the central Scandian Caledonides. In: Gee, D.G., Sturt, B.A. (eds), The Caledonide Orogen – Scandinavia and related areas. Wiley, Chichester, 953-970.

Stephens, M.B., and Gee, D.G., 1989. Terranes and polyphase accretionary history in the Scandinavian Caledonides. In: Dallmeyer, R.D. (ed.) Terranes in the Circum-Atlantic Paleozoic Orogens, Geological Society of America Special Papers, 230, 17-30.

Sundvoll, B. & Roberts, D., 2003. A likely Ordovician age for the regional, penetrative cleavage in the Gaissa Nappe Complex, northern Norway. Norges Geologiske Undersøkelse Bulletin, 441, 51–59.

Tajcmanova, L., Connolly, J.A.D., Cesare, B., 2009. A thermodynamic model for titanium and ferric iron solution in biotite. Journal of Metamorphic Geology 27, 153-165.

Townsend, C., Rice, A.H.N., and Mackay, A., 1989. The structure and stratigraphy of the southwestern portion of the Gaissa thrust belt and the adjacent Kalak Nappe Complex, north Norway. In: Gayer, R.A. (ed.) The Caledonide Geology of Scandinavia. Graham and Trotman, London, 111-126.

Wakabayashi, J., 2004. Tectonic mechanisms associated with P-T paths of regional metamorphism: alternatives to singe-cycle thrusting and heating, Tectonophysics, 392, 193-218.

Wei, C.J. & Powell, R., 2003. Phase relations in high-pressure metapelites in the system KFMASH (K_2O-FeO-MgO-Al_2O3-SiO_2-H_2O) with applications to natural rocks. Contributions to Mineralogy and Petrology, 145, 301-315.

White, R.W., Powell, R. & Phillips, G.N., 2003. A mineral equilibria study of the hydrothermal alteration in mafic greenschist facies rocks at Kalgoorlie, Western Australia. Journal of Metamorphic Geology, 21, 455-468.

White, R.W., Powell, R., Holland, T.J.B., 2007. Progress relating to calculation of partial melting equilibria for metapelites. Journal of Metamorphic Geology 25, 511-527.

Whitney, D.L., and Evans, B.W., 2010. Abbreviations for names of rock-forming minerals, American Mineralogist, 95, 185-187.

Yin, A., and Harrison, M., 2000. Geologic evolution of the Himalayan-Tibet orogeny, Annual Review of Earth and Planetary Sciences, 28, 211-280.

Zeh, A., Holland, T.J.B., and Klemd, R., 2005. Phase relationships in grunerite–garnet-bearing amphibolites in the system CFMASH, with applications to metamorphic rocks from the Central Zone of the Limpopo Belt, South Africa, Journal of Metamorphic Geology, 23, 1-17.

Zhang, W., Roberts, D., and Pease, V., 2016. Provenance of sandstones from Caledonian nappes in Finnmark, Norway: implications for Neoproterozoic-Cambrian paleogeography, Tectonophysics, 691, 198-205.

Zwaan, K.B., 1988. Nordreisa, berggrunnsgeologisk kart – M 1:250 000. Norges geologiske unerdsøkelse.

Zwaan, B.K., and van Roermund, H.L.M., 1990. **A** rift-related mafic dyke swarm in the Corrovare Nappe of the Caledonian Middle Allochthon, Troms, North Norway, and its tectonometamorphic evolution, Norges Geologiske Bulleting, 419, 25-44.

Figure Captions

Figure 1: Map of northern Norway showing the extent of the KNC and the overlying and underlying units.

Figure 2: Map of the study area showing lithologies, structures, sample sites, and sites of interest. Eide lens and Sandøra are noted as the sites of two recent published studies in the area (Corfu et al., 2007; Gasser et al., 2015). A representative cross section across the middle of the field area shows the relationship between different units and nappes.

Figure 3: Field photographs of rocks from the lower units in the KNC. A) Typical granodioritic orthogneiss in the lower KNC with a greenschist facies overprint (chlorite and muscovite) from the western side of Reisafjord. B) Amphibolite fold at site ST257. The S2 foliation comprises the sheared lower limb (garnet-bearing) of the fold with the S1 foliation (epidote, no garnet) in the hinge zone. C) Folded amphibolite and garnet-mica-schist from site S8d on Skjervøy. D) Panoramic photograph of the outcrop along southern Straumfjord showing an S1 low-strain lens and contacts between the amphiboltite and hbl-schist unit (Amp) and orthogneiss unit (Or). The boundaries between the two units are marked in black. Foliation in the orthogneiss is shown in light (S1) and dark (S2) blue, and foliation in the amphibolites is shown in orange (S1) and red (S2). E) Mylonitic (S2) meta-arkose with sheared amphibolite layer (sheared dyke) from Skjervøy at N70.030292°, E20.997759°. F) Felsic granite crosscutting folded foliation (S1) in meta-arkose on Skjervøy at N70.019598°, E20.993102°. G) Mafic dyke crosscutting early S1 foliation in meta-arkose on Skjervøy at N70.029047°, E21.00409°.

Figure 4: Tectonostratigraphy of the Kalak Nappe Complex including representative columns from Straumfjord, Hamneide, Eide, Uløya, Taskeby, Kågen, Skjervøy, and Arnøya. Based on Zwaan (1988) and own work. Tectonostratigraphic position of the investigated samples and sites of interest (Sandøra and Eide lens; Corfu et al., 2007; Gasser et al., 2015) are indicated.

Figure 5: Field photographs of rocks from the upper part of the KNC. A) Typical sheared paragneiss observed throughout the upper KNC, from Eide at N69.903898°, E020.922038°. B) Edge of a migmatitic gneiss (Sandøra) lens in the paragneisses on southern Skjervøy at N70.006°, E020.92549°. C) A mylonitic garnet amphibolite layer with sheared felsic layers in the paragneisses on southwestern Arnøya at N70.062744°, E20.46114°. D) Garnet amphibolite within the paragneisses at Eide (N69.88851°, E20.92265°) in a lower strain zone, showing a tight fold with a shallowly SE-dipping axial plane. E) Typical sheared meta-arkose unit from the upper Kalak with sheared quartz-feldspar lenses, at N69.996416°, E021.033235° on Taskeby. F) A small lower strain lens in metapsammitic paragneiss on the Eide Peninsula (N69.903898°, E020.922038°) showing cm-scale folding of an S1 foliation surrounded by S2 mylonite.

Figure 6: Equal area lower hemisphere stereonets showing poles to S1 foliation (orange), poles to S2 foliation (red), L1 mineral lineation (green), L2 stretching lineation (blue), small fold hinges (open circles), and poles to fold axial planes (black boxes) in the KNC. A) The relationship between older lower grade ($S1^S$, L1) and younger higher grade (S2, L2) structures is best observed in Straumfjord where S1 structures are more prevalent. B) The lower units in Skjervøy show a consistent S2 foliation and associated L2 lineation with rare earlier structures. C) The upper unit (paragneiss) on Skjervøy displays more variation in S2 and L2 structures and the $S1^E$ foliation is present as a high-grade migmatitic foliation within preserved lenses. D) In the Eide area an S1 foliation is also present in $S1^E$ lenses in the paragneisses and the structures display a similar relationship as the upper unit on Skjervøy. Small fold hinges trend more southward. E) The KNC on Uløya displays a dominant S2 foliation with few instances of earlier S1 foliation. Fold hinges trend mostly SE, but vary between SW, SE and E. Fold axial planes are shallow and parallel to S2. F) The KNC on Arnøya displays a pervasive S2 foliation with associated NW-SE trending stretching lineation.

Figure 7: Photomicrographs in plain (PPL) and cross (XPL) polarized light showing mineralogy and microstructures. A) Amphibolite sample ST254b with the $S1^S$ foliation

defined by amphibole, qtz ribbons, epidote and titanite (PPL). Calcite is found as late crosscutting grains. B) Photomicrograph (XPL) of sample ST257 showing three euhedral garnet grains in a matrix of amphibole, plagioclase, quartz and calcite. Amphibole defines the S2 foliation. Calcite occurs both in the matrix and as inclusions in garnet rims. C) Garnet grain in sample ST257 showing clinopyroxene and ilmenite as inclusions (PPL). D) Inclusions in garnet from sample S8d showing evidence for a pre-tectonic foliation defined by chlorite, biotite, ilmenite and quartz inclusions (PPL). Muscovite anastomoses around garnet grains. E) Interconnected muscovite and polymineralic quartz ribbons define a strong S2 foliation in sample S8d (XPL). Rutile is also present parallel to the S2 foliation. F) Garnet in sample S174a shows fine-grained inclusions in their cores with larger inclusions in the rims (PPL). Chlorite is common as larger inclusions towards the rims. G) The S2 foliaiton in sample S174a is defined by partially interconnected biotite and elongate quartz and feldspar grains (XPL). Titanite forms euhedral grains parallel to S2. H) Fine-grained kyanite and muscovite form along boundaries between garnet and staurolite (PPL) in sample S17. Muscovite, quartz and rutile also occur. I) Kyanite also occurs as large grains in sample S17 and shows large quartz and rutile inclusions (PPL). J) Garnet in sample UL250 shows cores with minor small inclusions and rims with abundant titanite and quartz inclusions (XPL). Titanites form a pattern indicating they probably grew during rotation of garnet. Biotite is interconnected and overgrows muscovite. It defines a strong S2 foliation. K) Large garnets in sample AR186 show chlorite and quartz inclusions in their cores and biotite inclusions towards their rims (PPL). L) The matrix of sample AR186 is mainly comprised of plagioclase and K-feldspar (XPL). Biotite forms isolated grains and late fine-grained muscovite occurs at K-feldspar boundaries.

Figure 8: BSE images and garnet profiles for samples ST257, S8d and S174a. A) Garnet in sample ST257 is euhedral with inclusion-rich cores. The profile displays a steady decrease of Sps and slight and steady increase in Py, Grs and Alm towards rims. B) Inclusions in garnet show evidence for a pre-tectonic foliation. A profile perpendicular to the early foliation displays a difference within a distinctive zone containing less inclusions, with higher Grs and X_{Mg} values and lower Alm. The shape of the Sps profile is

different and peak Sps values are highest in the centre of the garnet and gradually decrease towards rims. C) Garnet microstructure in sample S174a shows distinctive core and rim zones. Garnet cores display low Sps and Grs and high Alm, X_{Mg} and Py contents. Mid-garnet Sps and Grs values increase to their peaks and X_{Mg}, Py and Alm decrease to their lowest values. Towards garnet rims Sps values drop again, whereas Grs values drop only slightly. Alm, Py and X_{Mg} values increase back up to approximately the same as core values.

Figure 9: Map, BSE images and garnet profiles for samples S17, UL250 and AR186. A) Although garnet microstructure in sample S17 shows distinct cores and rims, profiles are relatively flat for Alm, Grs, X_{Mg}, Sps and Py values. B) Map of Sps content in garnet and garnet profiled displays three different zones in garnet. The central part of the garnet displays variation mainly in Sps, with the highest values forming several peaks. Py and X_{Mg} show a slight decrease where Sps is high. Alm is lower in the core relative to rims, and Grs shows a relatively flat profile in the cores. A thin rim zone shows decreased Sps, slightly decreased Alm, and the same Grs, X_{Mg} and Py values as cores. C) Garnets in sample AR186 display distinctive cores and rims, although the profile only reflects a difference in Sps content. Sps content is higher in cores, decreases fairly sharply at the core-rim boundary, and then displays a relatively flat profile towards garnet edges. X_{Mg}, Py, Grs and Alm values all show relatively flat profiles.

Figure 10: Pseudosections for garnet amphibolite samples ST254b and ST257, representative of $S1^S$ and S2 foliations, respectively. A) P-T conditions are constrained by the mineral assemblage to the phase fields including Grt-Bt-Amp-Amp-Pl-Ilm-Zo-Sph-Qtz at 530 – 570 °C and 8.2 – 9.3 kbar. B) Measured garnet core compositions for sample ST257 agree with modelled compositions in the phase field Grt-Bt-Amph-Pl-Ilm-Cpx-Qtz at 675 – 690 °C and 8.3- 9 kbar. Garnet rim compositions agree with modelled isopleths in the phase fields Grt-Bt-Pl-Ilm-Cc-Qtz±Cpx at 650-670 °C and 10.8 – 12.3 kbar.

Figure 11: Pseudosections for samples S8d, S174a and UL250. A) Measured garnet core compositions for sample S8d agree with modelled compositions in the Grt-Bt-Chl-Ms-Pg-

Ilm-Qtz phase field. Garnet rim compositions agree with modelled isopleths with Grt-Bt-Pl-Ms-Rt-Qtz stable. B) Pseudosection for sample S174a showing stable mineral assemblages, modelled garnet modal% and P-T estimates from garnet compositions in Fig. B. C) Pseudosection for sample S174a contoured for X_{Mg}, Grs, and Sps compositions in garnet. Measured garnet compositions corresponding to garnet cores, mid-garnet and garnet rims are plotted constrain initial high-temperature, low-pressure conditions followed by cooling and then an increase in P-T during S2 shearing. D) The lack of biotite and plagioclase in the sample, together with the correspondence of modelled X_{Mg}, Grs and Sps garnet isopleths with measured values constrain peak metamorphism with Ms-Grt-Ky-Pg-Rt-Qtz stable.

Figure 12: Pseudosections for upper KNC sample UL250 and Vaddas-KNC boundary sample AR186. A) Pseudosection for sample UL250 shows peak metamorphism recorded by garnet rims in the phase field Grt-Bt-Pl-Rt-Qtz. Abundant titanite and zoisite in the matrix and chlorite inclusions in garnet record metamorphism along a path represented by the black arrow. B) Garnet core and rim compositions in sample AR186 constrain initial metamorphism in the rutile-bearing phase field followed by slightly higher pressure conditions in the titanite-bearing phase field.

Figure 13: A) P-T summary for metamorphism in the KNC showing S1 and S2 estimates. All samples from the lower-nappe in the KNC are shown in a blue-green colour scheme, all those from the upper nappe are shown in grey-scale colours, and the KNC upper boundary is shown in pink. All estimates for peak S2 shearing are shown as solid boxes, while earlier estimates either from preserved S1 foliation or from garnet cores are shown with outlines. B) Relative difference in S2 temperature with respect to tectonostratigraphic level. Ranges for estimates are shown as solid boxes with potential error (standard error of ± 50 °C) as lines. C) Relative difference in peak S2 pressure with respect to tectonostratigraphic level. Ranges for estimates are shown as solid boxes with potential error (standard error of ± 0.5 kbar) as lines.

Figure 14: Summary of ages and metamorphic conditions in the KNC including P-T estimates from this paper and ages and P-T estimates from previous literature, including: Elvevold et al., (1994), Kirkland et al., (2005, 2007a, 2007b, 2008a, 2008b), Slagstad et al., (2006), Roberts et al., (2006, 2010), Corfu et al., (2007, 2011), Gasser et al., (2015), and Gee et al., (2017). Coloured boxes denote P-T estimates from this work, and colours correspond to the colours used for samples in Figure 13. Where boxes are more than one colour, the estimate comes from more than one sample, of the corresponding colours in Figure 13.

Table captions

Table 1: List of samples showing sample locations and mineral assemblages. Minerals that only occur as inclusions in garnet are indicated.
Table 2: Bulk rock compositions from whole rock XRF analysis used for phase equilibrium modelling.
Table 3: Representative garnet analyses showing re-calculated garnet compositions on the basis of 8 cations and 12 oxygens.
Table 4: Representative mineral composition analyses for plagioclase, biotite and white mica.

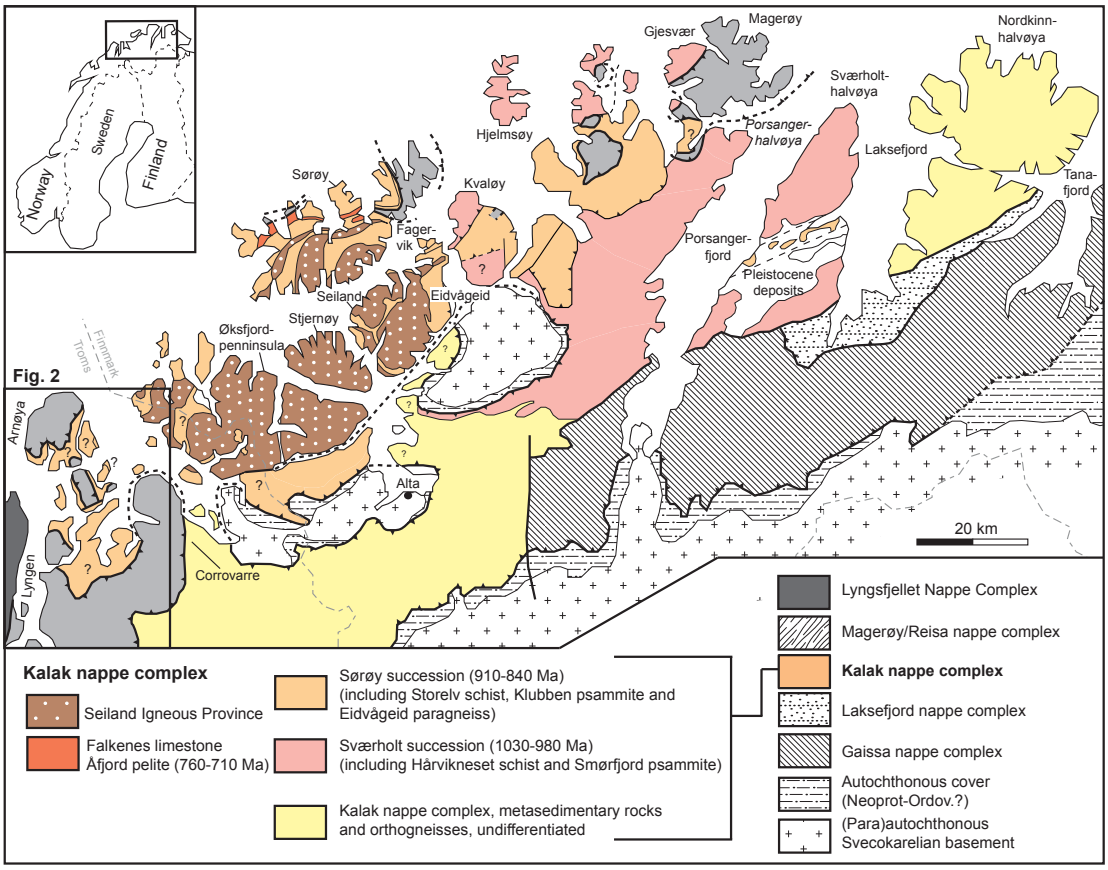
Norway
Sweden
Finland
Fig. 2
Finnmark
Troms
Magerøy
Gjesvær
Nordkinn-
halvøya
Sværholt-
halvøya
Hjelmsøy
Porsanger-
halvøya
Laksefjord
Tana-
fjord
Sørøy
Kvaløy
Fager-
vik
Porsanger-
fjord
Pleistocene
deposits
Seiland
Eidvågeid
Stjernøy
Øksfjord-
penninsula
Arnøya
Alta
Lyngen
Corrovarre
20 km
Kalak nappe complex
Seiland Igneous Province
Falkenes limestone
Åfjord pelite (760-710 Ma)
Sørøy succession (910-840 Ma)
(including Storelv schist, Klubben psammite and
Eidvågeid paragneiss)
Sværholt succession (1030-980 Ma)
(including Hårvikneset schist and Smørfjord psammite)
Kalak nappe complex, metasedimentary rocks
and orthogneisses, undifferentiated
Lyngsfjellet Nappe Complex
Magerøy/Reisa nappe complex
Kalak nappe complex
Laksefjord nappe complex
Gaissa nappe complex
Autochthonous cover
(Neoprot-Ordov.?)
(Para)autochthonous
Svecokarelian basement

Fig. 1

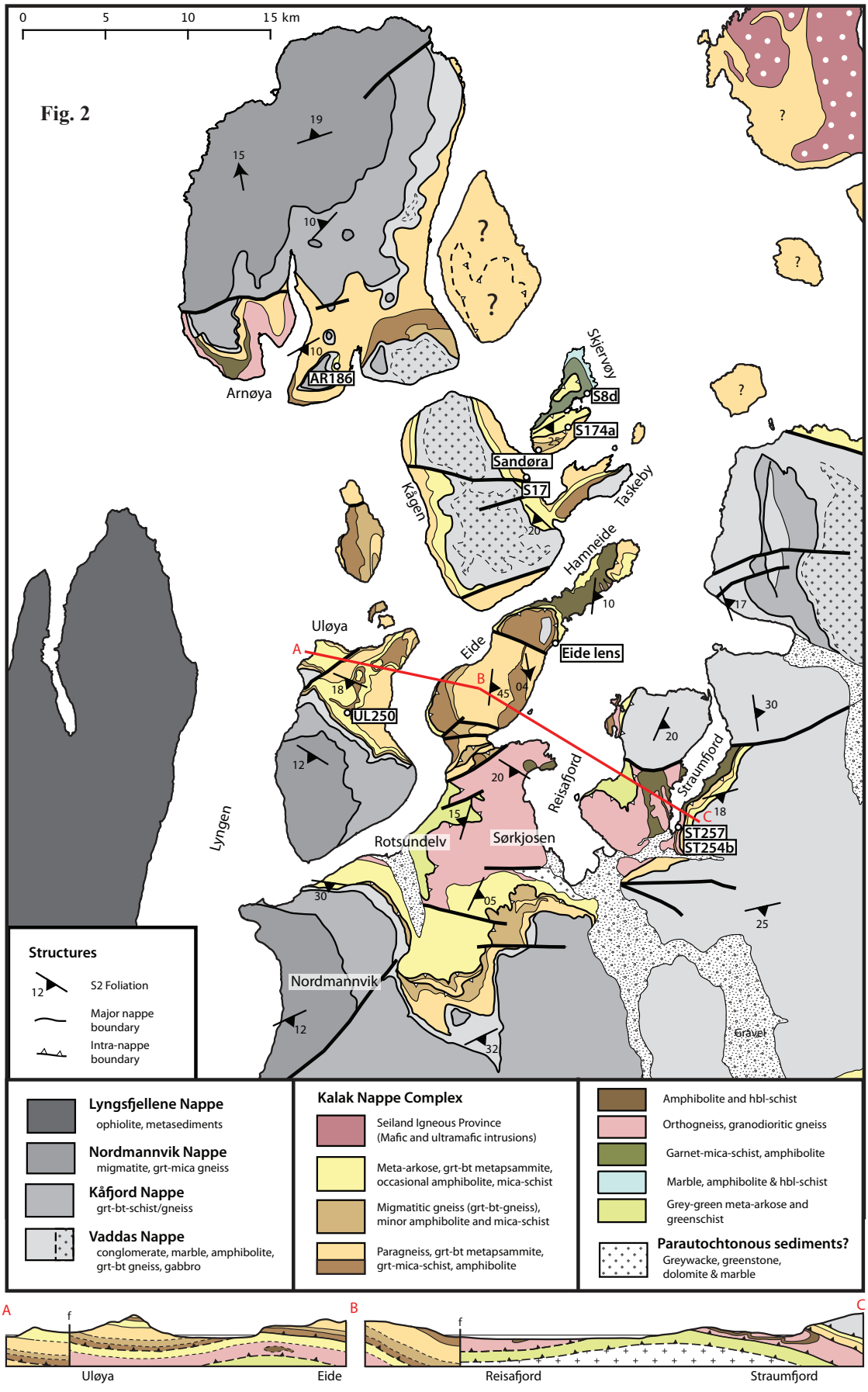
Fig. 2
0
5
10
15 km
Arnøya
AR186
Skjervøy
S8d
S174a
Sandøra
S17
Kågen
Taskeby
Hamneide
Uløya
Eide
Eide lens
A
B
C
UL250
Lyngen
Rotsundelv
Sørkjosen
Reisafjord
Straumfjord
ST257
ST254b
Nordmannvik
Gravel
Structures
S2 Foliation
Major nappe boundary
Intra-nappe boundary
Lyngsfjellene Nappe
ophiolite, metasediments
Nordmannvik Nappe
migmatite, grt-mica gneiss
Kåfjord Nappe
grt-bt-schist/gneiss
Vaddas Nappe
conglomerate, marble, amphibolite, grt-bt gneiss, gabbro
Kalak Nappe Complex
Seiland Igneous Province (Mafic and ultramafic intrusions)
Meta-arkose, grt-bt metapsammite, occasional amphibolite, mica-schist
Migmatitic gneiss (grt-bt-gneiss), minor amphibolite and mica-schist
Paragneiss, grt-bt metapsammite, grt-mica-schist, amphibolite
Amphibolite and hbl-schist
Orthogneiss, granodioritic gneiss
Garnet-mica-schist, amphibolite
Marble, amphibolite & hbl-schist
Grey-green meta-arkose and greenschist
Parautochtonous sediments?
Greywacke, greenstone, dolomite & marble
A
B
C
f
Uløya
Eide
Reisafjord
Straumfjord

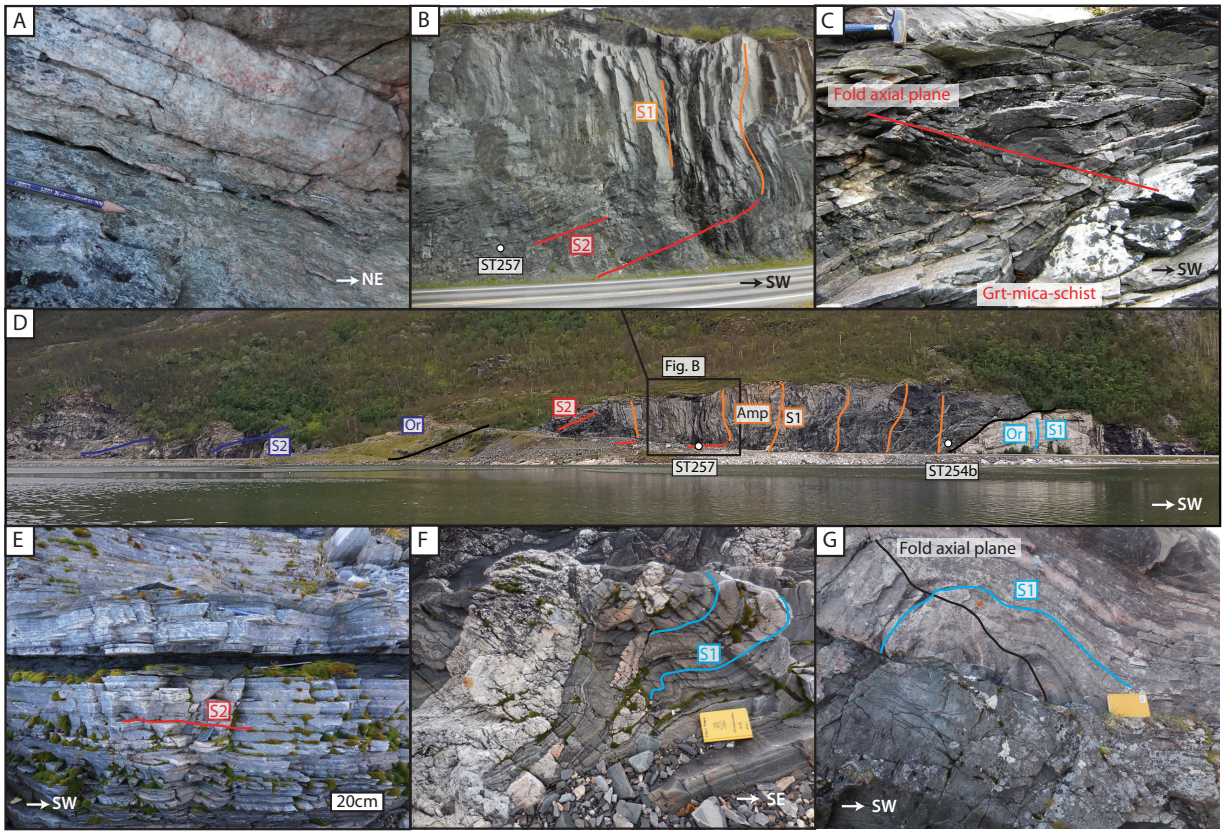
A
NE
B
S1
S2
ST257
SW
C
Fold axial plane
Grt-mica-schist
SW
D
Fig. B
S2
Or
S2
Amp
S1
ST257
ST254b
Or
S1
SW
E
S2
SW
20cm
F
S1
SE
G
Fold axial plane
S1
SW

Fig. 3

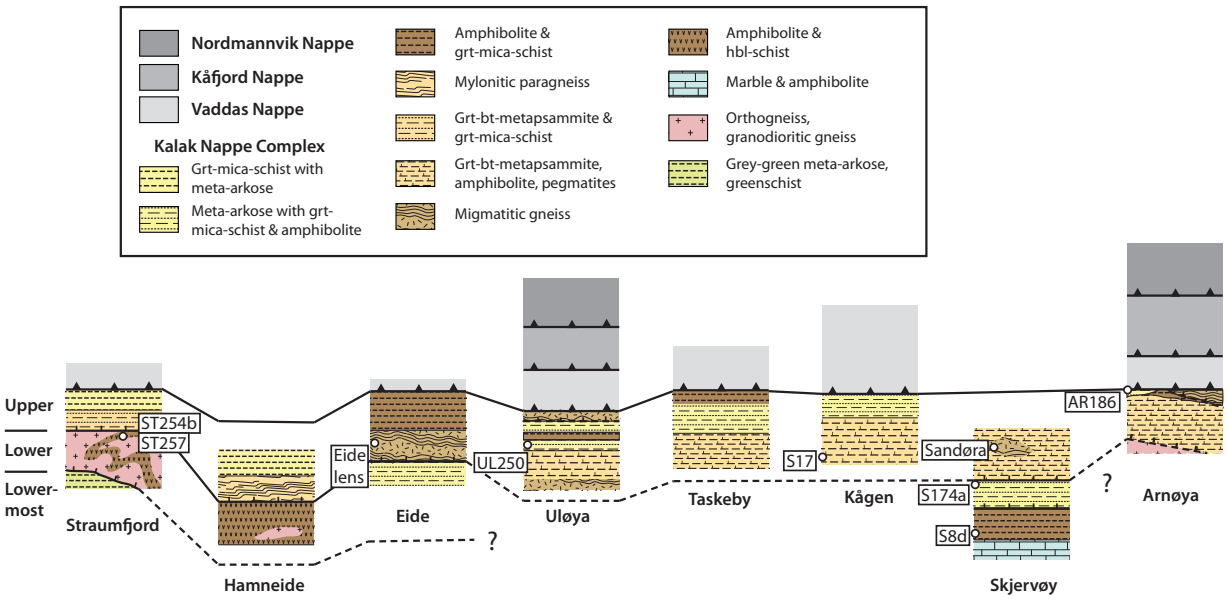
Nordmannvik Nappe
Kåfjord Nappe
Vaddas Nappe
Kalak Nappe Complex
Grt-mica-schist with meta-arkose
Meta-arkose with grt-mica-schist & amphibolite
Amphibolite & grt-mica-schist
Mylonitic paragneiss
Grt-bt-metapsammite & grt-mica-schist
Grt-bt-metapsammite, amphibolite, pegmatites
Migmatitic gneiss
Amphibolite & hbl-schist
Marble & amphibolite
Orthogneiss, granodioritic gneiss
Grey-green meta-arkose, greenschist
Upper
Lower
Lower-most
ST254b
ST257
Straumfjord
Hamneide
Eide lens
Eide
UL250
Uløya
?
Taskeby
S17
Kågen
Sandøra
S174a
S8d
Skjervøy
AR186
?
Arnøya

Fig. 4

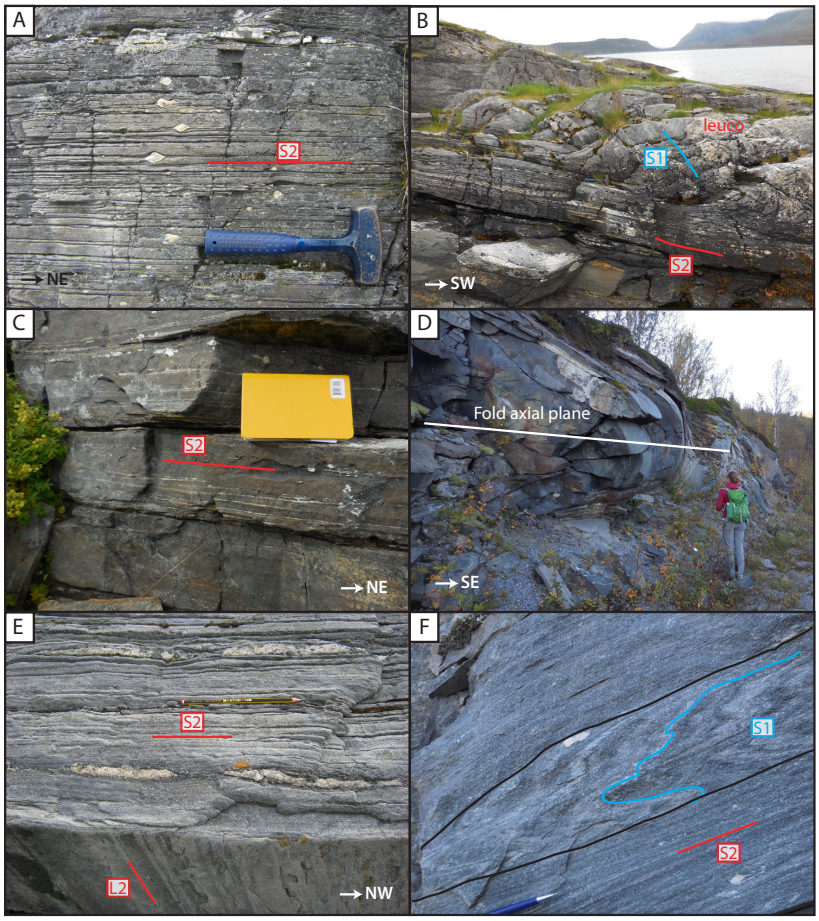
A
S2
NE
B
leuco
S1
S2
SW
C
S2
NE
D
Fold axial plane
SE
E
S2
L2
NW
F
S1
S2

Fig. 5

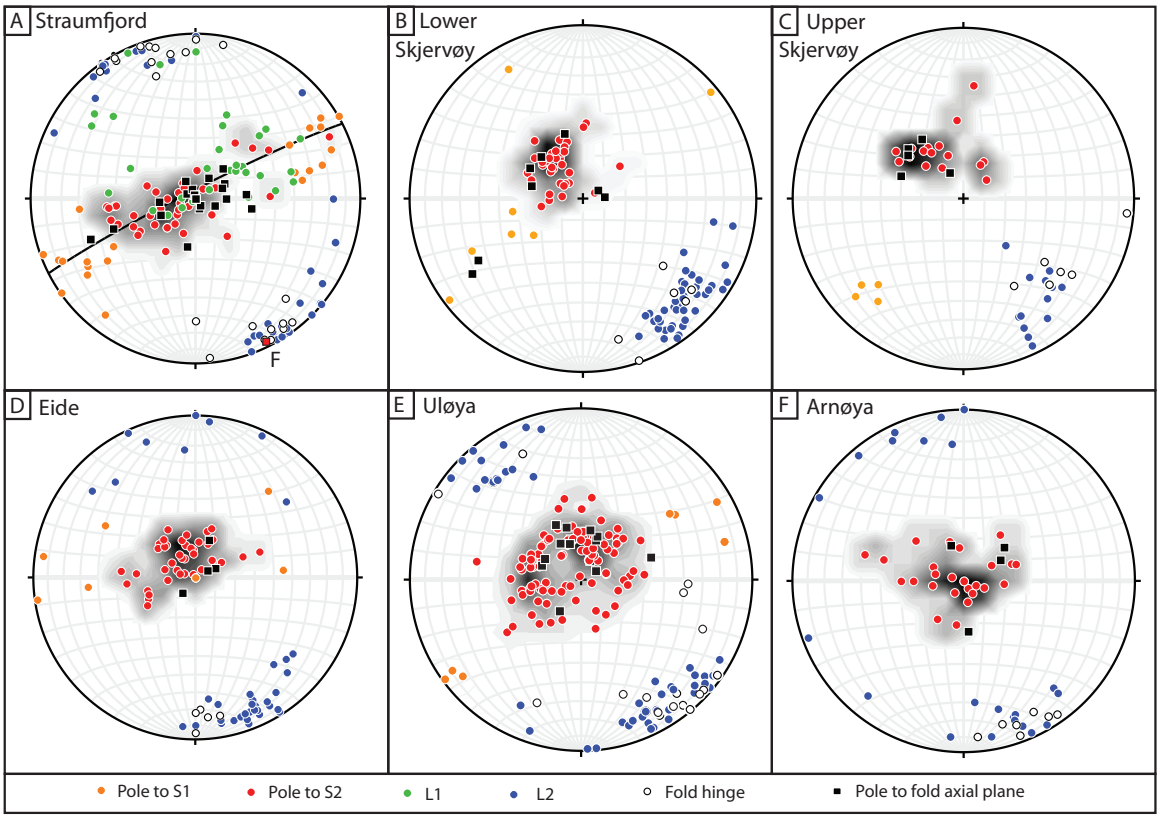
A Straumfjord
F
B Lower Skjervøy
C Upper Skjervøy
D Eide
E Uløya
F Arnøya
Pole to S1
Pole to S2
L1
L2
Fold hinge
Pole to fold axial plane

Fig. 6

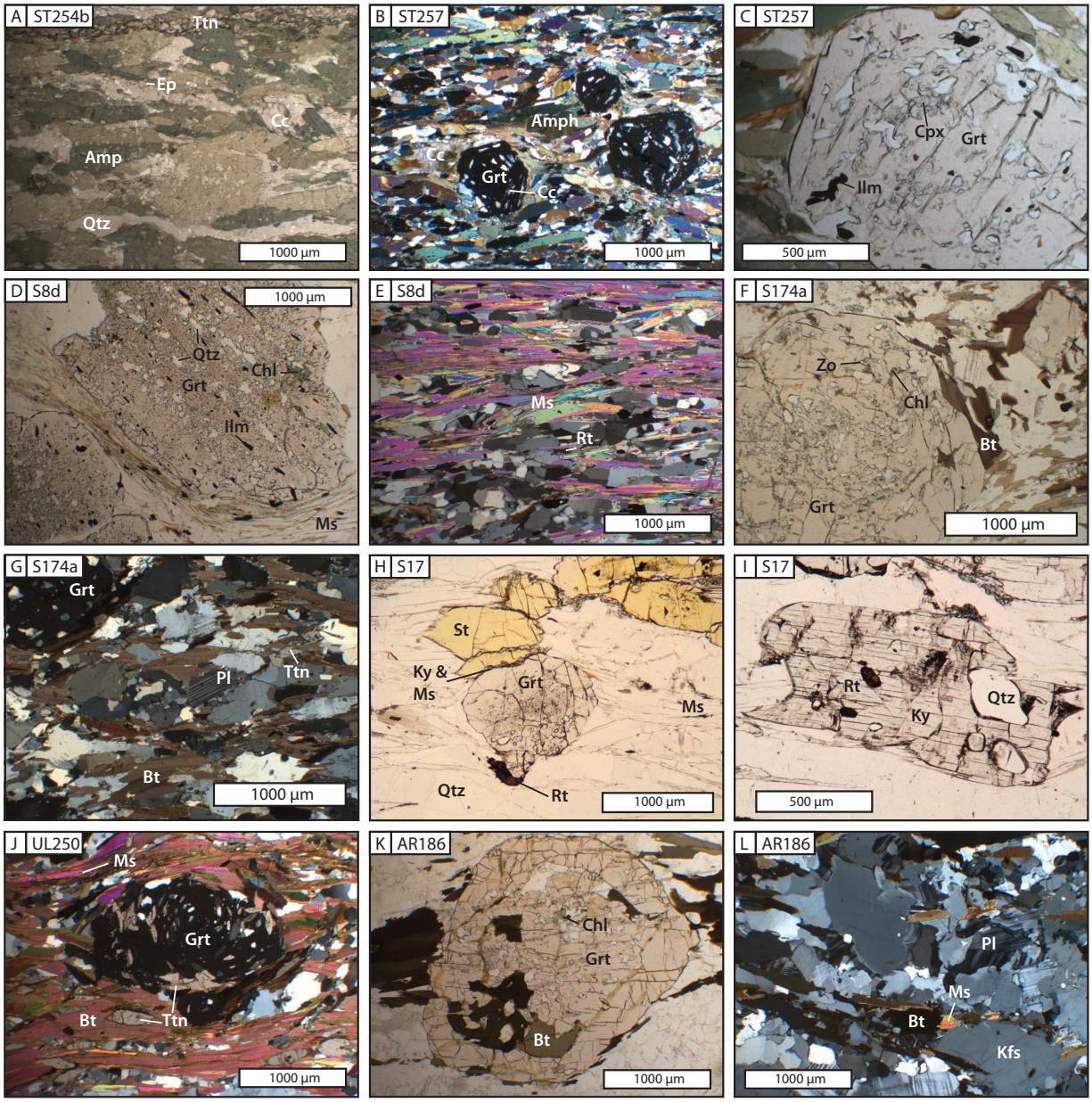
A ST254b
Ttn
Ep
Cc
Amp
Qtz
1000 µm
B ST257
Amph
Cc
Grt
Cc
1000 µm
C ST257
Cpx
Grt
Ilm
500 µm
D S8d
1000 µm
Qtz
Chl
Grt
Ilm
Ms
E S8d
Ms
Rt
1000 µm
F S174a
Zo
Chl
Bt
Grt
1000 µm
G S174a
Grt
Pl
Ttn
Bt
1000 µm
H S17
St
Ky &
Ms
Grt
Ms
Qtz
Rt
1000 µm
I S17
Rt
Qtz
Ky
500 µm
J UL250
Ms
Grt
Bt
Ttn
1000 µm
K AR186
Chl
Grt
Bt
1000 µm
L AR186
Pl
Ms
Bt
Kfs
1000 µm

Fig. 7

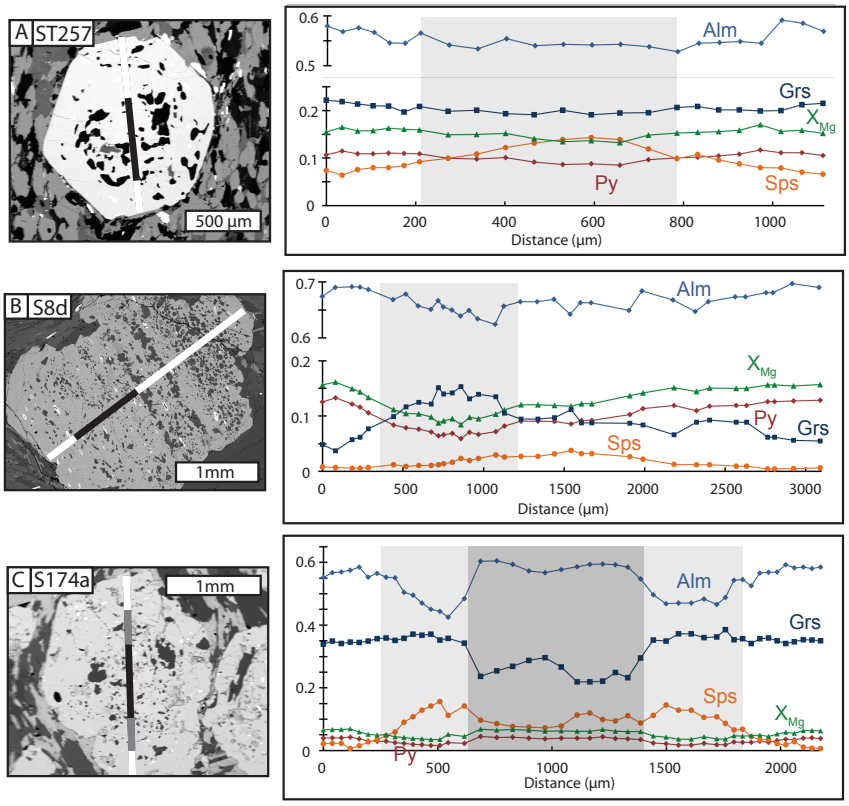
A ST257
500 µm
Alm
Grs
X_{Mg}
Py
Sps
Distance (µm)
B S8d
1mm
Alm
X_{Mg}
Py
Grs
Sps
Distance (µm)
C S174a
1mm
Alm
Grs
Sps
X_{Mg}
Py
Distance (µm)

Fig. 8

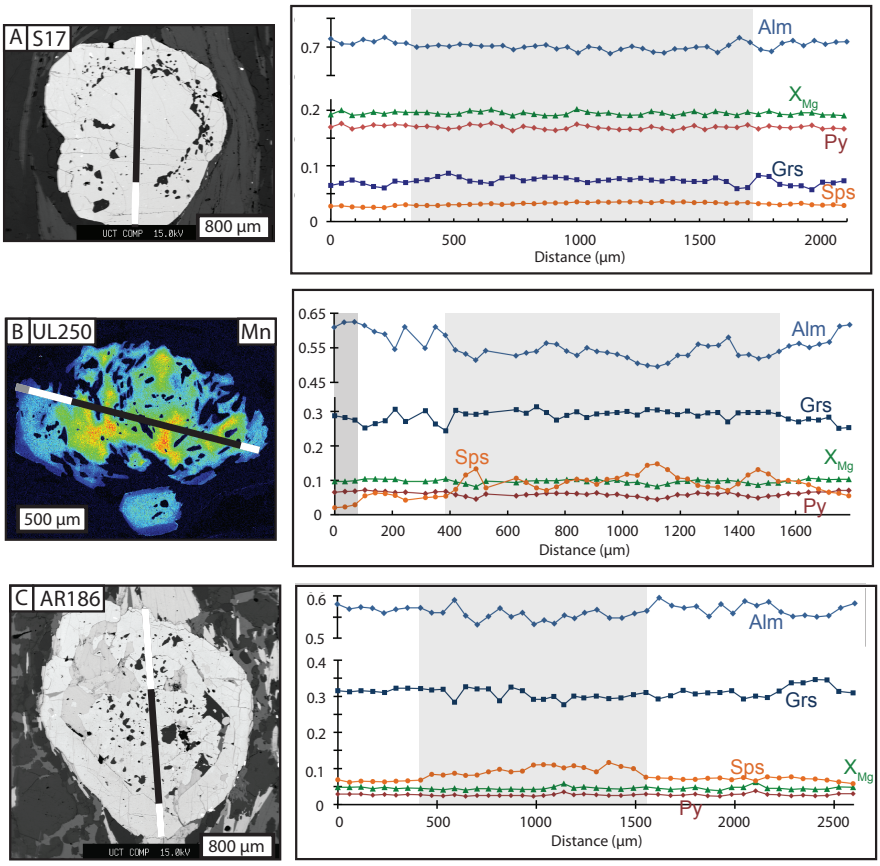
A S17
800 µm
Alm
X_{Mg}
Py
Grs
Sps
Distance (µm)
B UL250
Mn
500 µm
Alm
Grs
Sps
X_{Mg}
Py
Distance (µm)
C AR186
800 µm
Alm
Grs
Sps
X_{Mg}
Py
Distance (µm)

Fig. 9

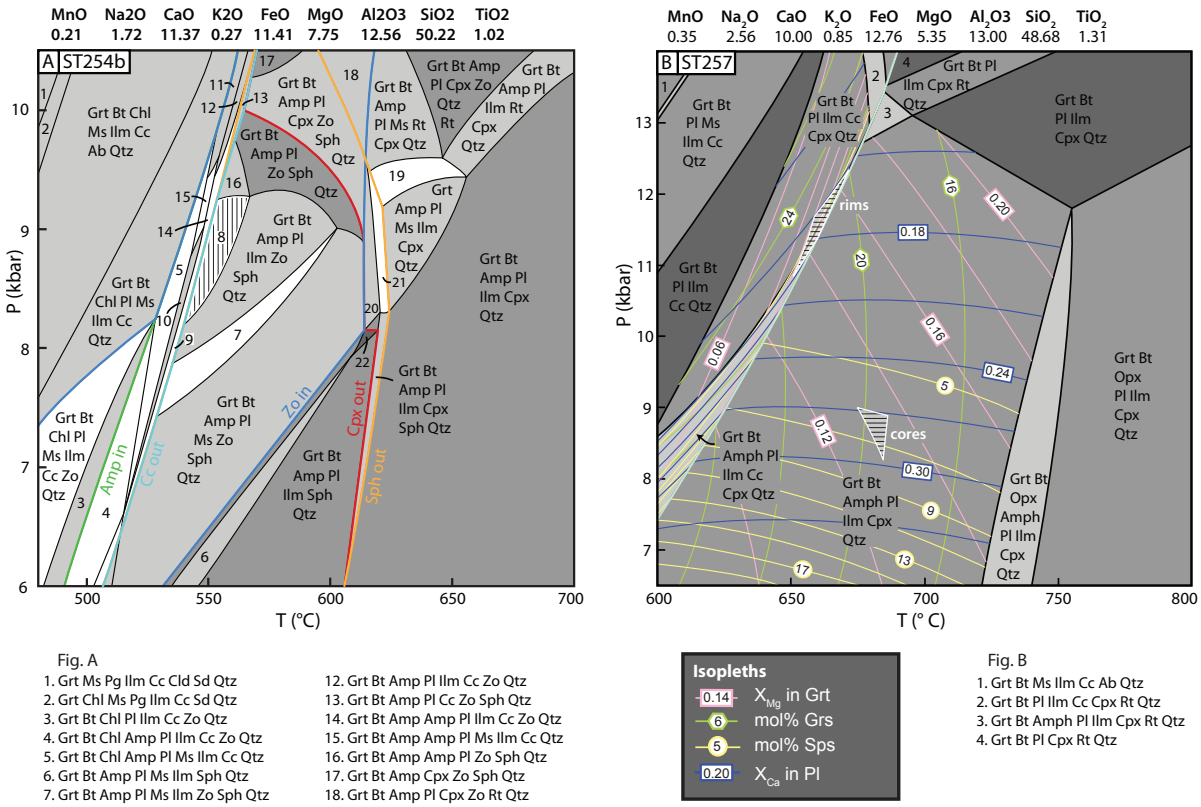

Fig. A

1. Grt Ms Pg Ilm Cc Cld Sd Qtz
2. Grt Chl Ms Pg Ilm Cc Sd Qtz
3. Grt Bt Chl Pl Ilm Cc Zo Qtz
4. Grt Bt Chl Amp Pl Ilm Cc Zo Qtz
5. Grt Bt Chl Amp Pl Ms Ilm Cc Qtz
6. Grt Bt Amp Pl Ms Ilm Sph Qtz
7. Grt Bt Amp Pl Ms Ilm Zo Sph Qtz
8. Grt Bt Amp Amp Pl Ilm Zo Sph Qtz
9. Grt Bt Amp Pl Ms Ilm Cc Zo Qtz
10. Grt Bt Amp Pl Ms Ilm Cc Qtz
11. Grt Bt Amp Pl Ms Ilm Cc Qtz
12. Grt Bt Amp Pl Ilm Cc Zo Qtz
13. Grt Bt Amp Pl Cc Zo Sph Qtz
14. Grt Bt Amp Amp Pl Ilm Cc Zo Qtz
15. Grt Bt Amp Amp Pl Ms Ilm Cc Qtz
16. Grt Bt Amp Amp Pl Zo Sph Qtz
17. Grt Bt Amp Cpx Zo Sph Qtz
18. Grt Bt Amp Pl Cpx Zo Rt Qtz
19. Grt Bt Amp Pl Ms Ilm Cpx Rt Qtz
20. Grt Bt Amp Pl Ms Gt Cpx Sph Qtz
21. Grt Bt Amp Pl Ms Ilm Cpx Sph Qtz
22. Grt Bt Amp Pl Sph Qtz

Fig. B

1. Grt Bt Ms Ilm Cc Ab Qtz
2. Grt Bt Pl Ilm Cc Cpx Rt Qtz
3. Grt Bt Amph Pl Ilm Cpx Rt Qtz
4. Grt Bt Pl Cpx Rt Qtz

Fig. 10

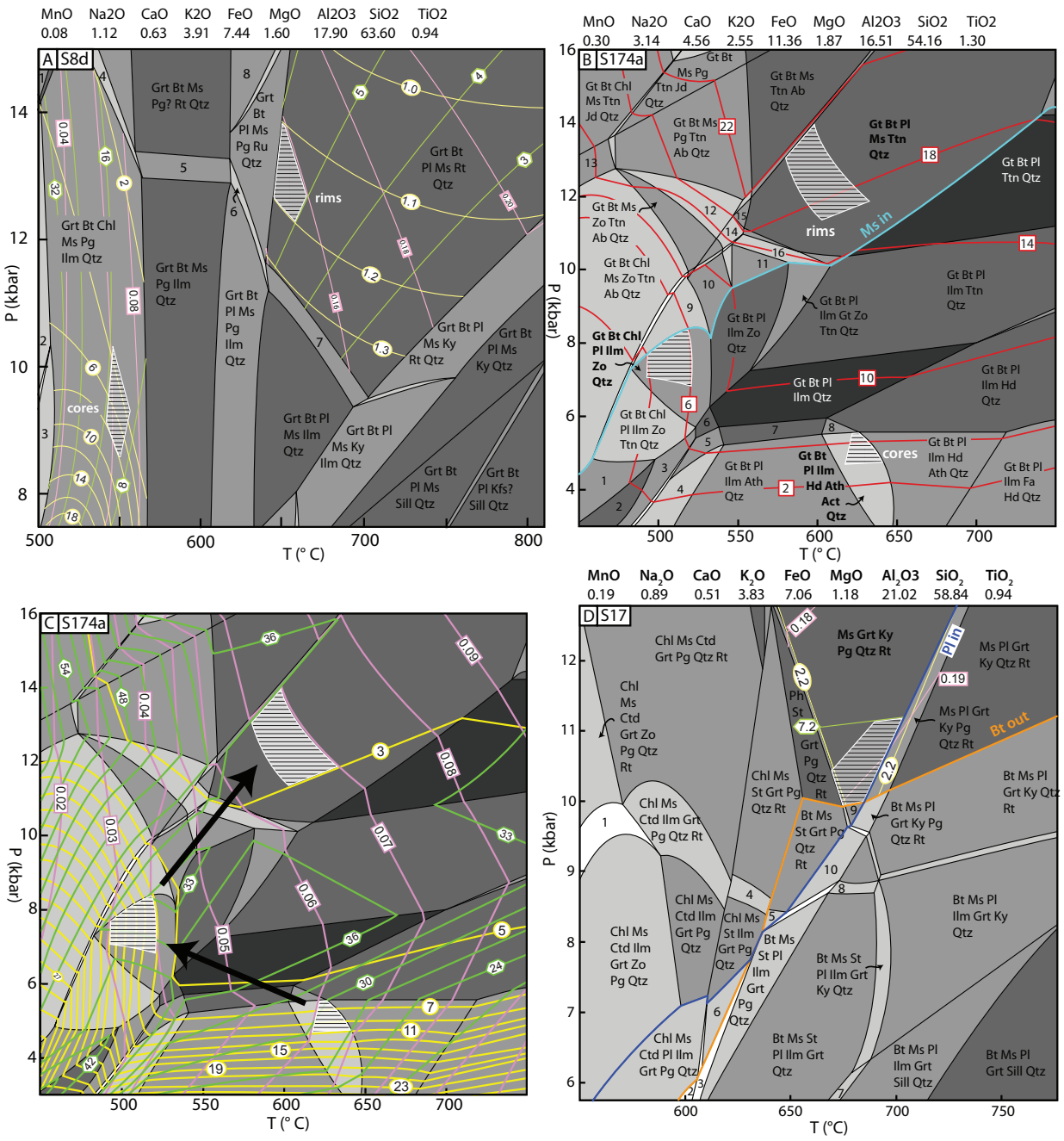

Fig. A

1. Grt Chl Ms Pg Rt Qtz
2. Grt Bt Chl Ms Pg Ilm Sph Qtz
3. Grt Bt Chl Ms Pg Ilm Zo Qtz
4. Grt Bt Chl Ms Pg Ilm Rt Qtz
5. Grt Bt Ms Pg Ilm Rt Qtz
6. Grt Bt Pl Ms Pg Ilm Rt Qtz
7. Grt Bt Pl Ms Ilm Rt Qtz
8. Grt Bt Ms Pg Ab Rt Qtz

Fig. B

1. Gt Bt Chl Pl Zo Ttn Qtz
2. Gt Bt Chl Pl Ttn Qtz
3. Gt Bt Chl Pl Ilm Ttn Qtz
4. Gt Bt Chl Pl Ilm Ath Act Qtz
5. Gt Bt Chl Pl Ilm Act Qtz
6. Gt Bt Chl Pl Ilm Qtz
7. Gt Bt Pl Ilm Act Qtz
8. Gt Bt Pl Ilm Hd Act Qtz
9. Gt Bt Chl Pl Ms Ilm Zo Qtz
10. Gt Bt Pl Pg Ilm Zo Qtz
11. Gt Bt Pl Ms Ilm Zo Qtz
12. Gt Bt Ms Pg Zo Ttn Ab Qtz
13. Gt Bt Chl Ms Ttn Ab Qtz
14. Gt Bt Pl Ms Pg Zo Ttn Qtz
15. Gt Bt Pl Ms Pg Ttn Qtz
16. Gt Bt Pl Ms Ilm Zo Ttn Qtz

Fig. D

1. Chl-Ms-Ctd-Ilm-Grt-Zo-Pg-Qtz-Rt
2. Bt-Chl-Ms-Ctd-Pl-Ilm-Grt-Pg-Qtz
3. Bt-Chl-Ms-St-Pl-Ilm-Grt-Pg-Qtz
4. Chl-Ms-St-Ilm-Grt-Pg-Qtz-Rt
5. Bt-Ms-St-Ilm-Grt-Pg-Qtz-Rt
6. Chl-Ms-St-Pl-Ilm-Grt-Pg-Qtz
7. Bt-Ms-St-Pl-Ilm-Grt-Sill-Qtz
8. Bt-Ms-St-Pl-Ilm-Grt-Qtz-Rt
9. Bt-Ms-Grt-Ky-Pg-Qtz-Rt
10. Bt-Ms-St-Pl-Grt-Pg-Qtz-Rt

Fig. 11

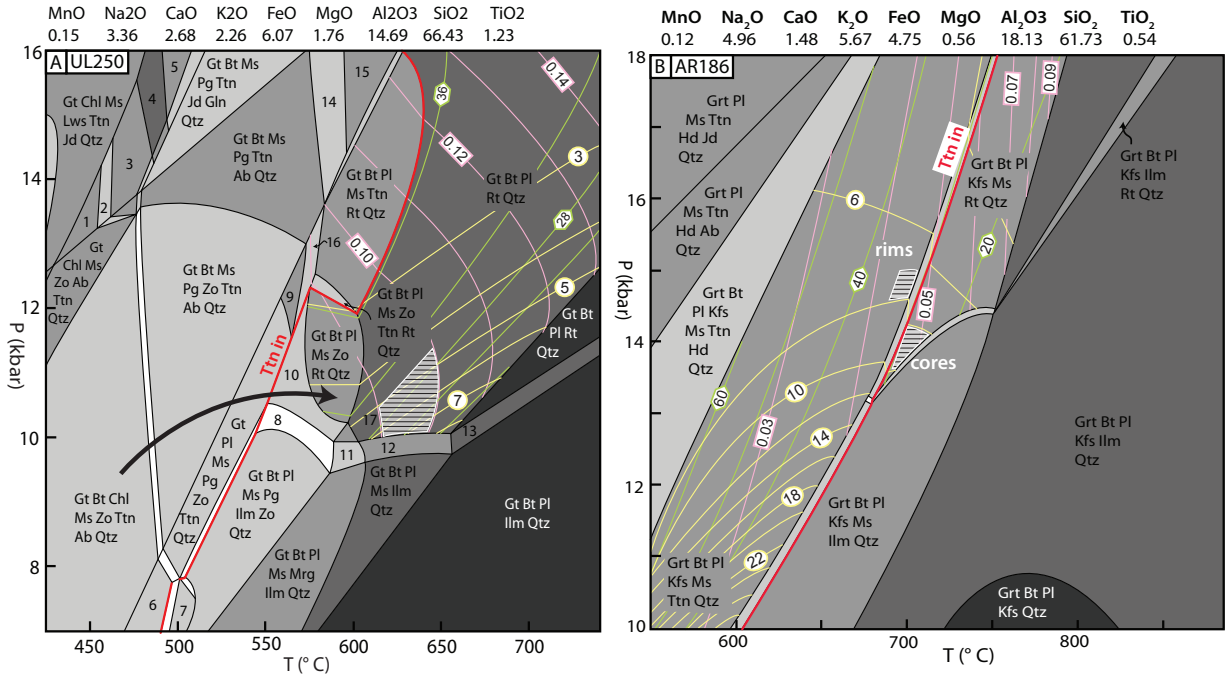

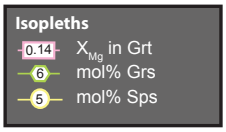

Fig. A

1. Gt Chl Ms Zo Ttn Jd Qtz
2. Gt Chl Ms Pg Gt Zo Ttn Jd Qtz
3. Gt Chl Ms Pg Ttn Jd Qtz
4. Gt Chl Ms Gt Ttn Jd Qtz
5. Gt Chl Ms Gt Ttn Jd Gln Qtz
6. Gt Bt Chl Pl Ms Zo Ttn Qtz
7. Gt Bt Chl Pl Ms Ilm Zo Qtz
8. Gt Bt Pl Ms Pg Ilm Zo Rt Qtz
9. Gt Bt Pl Ms Pg Ttn Qtz
10. Gt Bt Pl Ms Pg Zo Rt Qtz
11. Gt Bt Pl Ms Pg Ilm Rt Qtz
12. Gt Bt Pl Ms Ilm Rt Qtz
13. Gt Bt Pl Ilm Rt Qtz
14. Gt Bt Ms Pg Ttn Ab Rt Qtz
15. Gt Bt Ms Ttn Ab Rt Qtz
16. Gt Bt Pl Ms Pg Ttn Rt Qtz
17. Gt Bt Pl Ms Pg Rt Qtz

Fig. 12

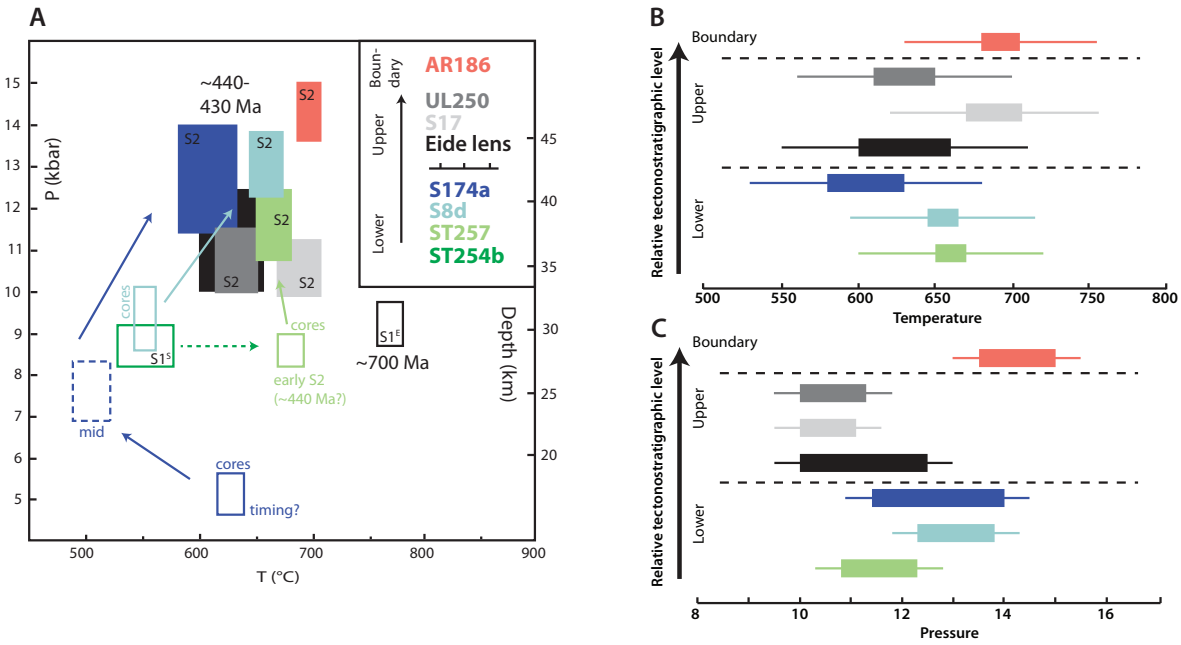
A
~440-
430 Ma
S2
S2
S2
S2
S2
S2
P (kbar)
T (°C)
Depth (km)
cores
S1ˢ
cores
early S2
(~440 Ma?)
mid
cores
timing?
S1ᵉ
~700 Ma
Boun-
dary
Upper
Lower
AR186
UL250
S17
Eide lens
S174a
S8d
ST257
ST254b
B
Boundary
Upper
Lower
Relative tectonostratigraphic level
Temperature
C
Boundary
Upper
Lower
Relative tectonostratigraphic level
Pressure

Fig. 13

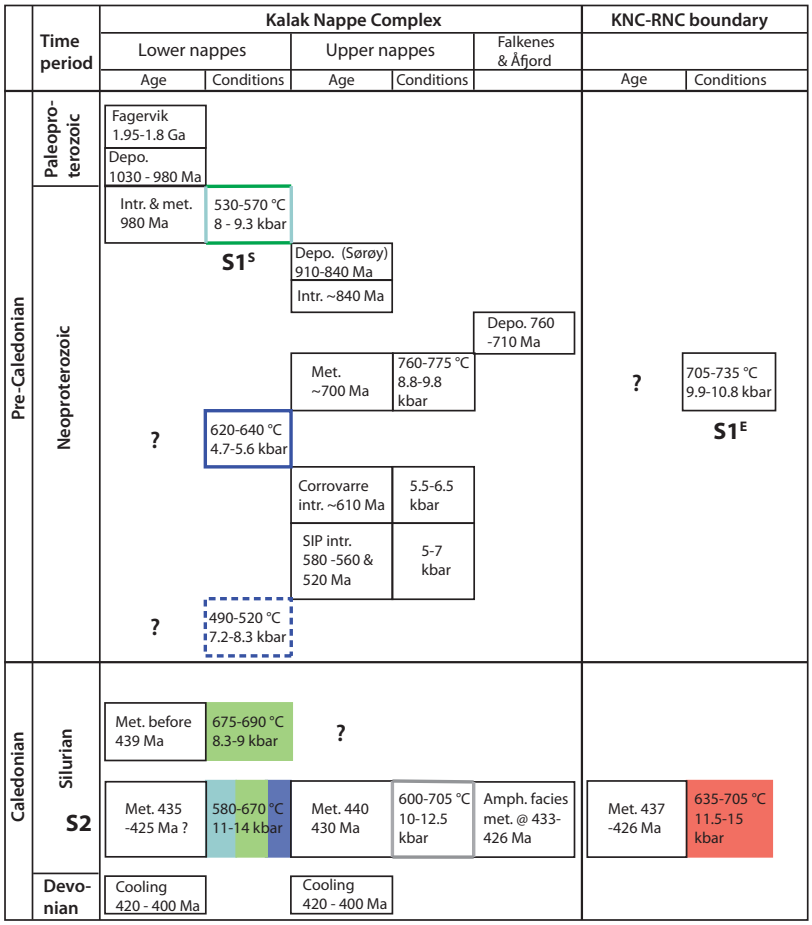
Time period
Kalak Nappe Complex
Lower nappes
Upper nappes
Falkenes & Åfjord
KNC-RNC boundary
Age
Conditions
Age
Conditions
Age
Conditions
Pre-Caledonian
Paleopro-terozoic
Neoproterozoic
Caledonian
Silurian
Devo-nian
S2
Fagervik 1.95-1.8 Ga
Depo. 1030 - 980 Ma
Intr. & met. 980 Ma
530-570 °C 8 - 9.3 kbar
S1S
Depo. (Sørøy) 910-840 Ma
Intr. ~840 Ma
Depo. 760 -710 Ma
Met. ~700 Ma
760-775 °C 8.8-9.8 kbar
?
620-640 °C 4.7-5.6 kbar
Corrovarre intr. ~610 Ma
5.5-6.5 kbar
SIP intr. 580 -560 & 520 Ma
5-7 kbar
?
490-520 °C 7.2-8.3 kbar
?
705-735 °C 9.9-10.8 kbar
S1E
Met. before 439 Ma
675-690 °C 8.3-9 kbar
?
Met. 435 -425 Ma ?
580-670 °C 11-14 kbar
Met. 440 430 Ma
600-705 °C 10-12.5 kbar
Amph. facies met. @ 433-426 Ma
Met. 437 -426 Ma
635-705 °C 11.5-15 kbar
Cooling 420 - 400 Ma
Cooling 420 - 400 Ma

Fig. 14

Table 1. Mineral assemblages and sample sites for all samples

			Main minerals												Accessory minerals						
Area	Sample	Site	Bt	Pl	Qtz	Grt	Kfs	St	Ky	Zo	Amph	Ms	Chl	Cc	Cpx	Zrn	Mnz	Rt	Ttn	Ill	Ap	Ep/All
Straumfjord	ST254b	N69.80727°, E21.14211°			x					x	x			x					x	x	x	x
Straumfjord	ST257	N69.80727°, E21.14211°	x	x	x	x					x			x	x (in.)			x		x	x	
Lower Skjervøy	S8d	N70.03757°, E21.00038°	x	x	x	x		x	x			x				x		x			x	
Upper Skjervøy	S174a	N70.01789°, E20.07538°	x	x	x	x						x				x		x	x		x	x
Kågen	S17	N69.99283°, E20.90679°			x	x				x (in.)			x(in.)						x	x (in.)	x	x
Uløya	UL250	N69.86851°, E20.6291°	x	x	x	x						x	x (in.)			x		x		x (in.)	x	
Vaddas-KNC boundary	AR186	N70.05338°, E20.60666°	x	x	x	x	x					x	x (in.)			x		x	x		x	x

Table 2: XRF bulk composition analyses for petrology samples

Sample	ST254b	ST257	S8d	S174a	S17	UL250	AR186
Na_2O	1.72	2.26	1.12	3.14	0.89	3.36	4.96
MgO	7.75	5.35	1.60	1.87	1.18	1.76	0.56
Al_2O_3	12.56	13.00	17.90	16.51	21.02	14.69	18.13
SiO_2	50.22	48.68	63.60	54.16	58.84	66.43	61.73
P_2O_5	0.09	0.11	0.19	0.88	0.17	0.32	0.26
K_2O	0.27	0.85	3.91	2.55	3.83	2.26	5.67
CaO	11.49	10.14	0.88	5.71	0.74	3.10	1.81
TiO_2	1.02	1.31	0.94	1.30	0.94	1.23	0.54
MnO	0.21	0.35	0.08	0.30	0.19	0.15	0.12
Fe_2O_3	12.68	14.17	8.27	12.63	7.85	6.74	5.27
Cr_2O_2	0.07	0.03	0.00	0.00	0.01	0.01	0.00
NiO	0.02	0.02	0.00	0.01	0.01	0.01	0.01
LOI	1.23	3.35	1.54	0.48	3.72	0.61	0.41
Total	99.33	99.61	100.03	99.53	99.40	100.65	99.47

Table 3: Representative garnet compositions

Grt																								
Sample	ST257				S8d				S174a				S17				UL250				AR186			
	Core	Rim	Core	Rim	Core	Rim	Core	Rim	Core	Rim	Core	Rim	Grt1 core	Grt1 rim	Grt2 core	Grt2 rim	Core	Rim	Core	Rim	Grt1 core	Grt1 rim	Grt2 core	Grt2 rim
Wt%																								
SiO_2	37.72	37.59	37.40	37.50	37.51	37.72	38.10	37.86	37.47	38.27	37.72	38.13	37.66	37.35	37.97	37.95	37.97	37.92	37.81	37.74	37.20	37.62	37.31	37.53
TiO_2	0.15	0.25	0.07	0.06	0.00	0.00	0.00	0.00	0.14	0.08	0.18	0.02	0.08	0.13	0.15	0.01	0.00	0.02	0.01	0.00	0.08	0.06	0.09	0.09
Al_2O_3	21.41	21.76	21.38	21.65	21.53	21.96	21.80	21.92	21.61	22.10	21.37	21.65	22.18	21.86	21.90	22.06	21.62	21.63	21.37	21.58	21.07	21.16	20.97	21.18
Fe_2O_3	0.27	0.57	0.76	0.63	0.00	0.00	0.00	0.00	0.39	0.00	0.10	0.00	0.00	0.00	0.00	0.00	0.00	0.00	0.00	0.00	0.00	0.00	0.00	0.00
FeO	24.94	26.71	25.08	26.35	30.71	34.52	32.86	35.05	26.91	25.78	20.75	26.99	32.22	32.00	32.12	31.61	27.59	22.86	23.05	28.22	24.90	26.08	24.75	26.04
MnO	5.83	3.50	6.56	2.94	2.70	0.42	1.51	0.38	5.13	1.03	7.36	0.58	1.36	1.19	0.96	1.15	1.21	5.88	5.90	0.99	4.93	2.88	4.68	2.78
MgO	2.64	2.88	2.29	2.98	1.51	3.42	2.79	3.64	1.01	1.03	0.40	1.11	4.33	4.24	4.27	4.34	1.68	1.20	1.27	1.70	0.73	0.68	0.71	0.67
CaO	7.43	7.64	6.92	7.92	5.56	1.95	3.89	1.50	7.87	12.37	12.77	12.38	2.38	2.64	2.26	2.64	10.36	11.07	10.65	9.97	10.66	11.17	10.27	11.35
Total	100.39	100.91	100.46	100.03	99.52	99.99	100.95	100.35	100.52	100.67	100.65	100.86	100.21	99.41	99.63	99.76	100.43	100.57	100.06	100.20	99.57	99.65	98.78	99.63
Si	2.9856	2.9587	2.97314	2.96874	3.029	3.017	3.021	3.018	2.982	3.013	2.988	3.001	2.981	2.979	3.024	3.014	3.003	2.999	3.007	2.994	2.985	3.011	3.018	3.004
Ti	0.00914	0.01486	0.00393	0.00348	0.000	0.000	0.000	0.000	0.008	0.005	0.011	0.001	0.005	0.008	0.009	0.000	0.000	0.001	0.000	0.000	0.005	0.004	0.005	0.005
Al	1.99752	2.01885	2.0034	2.02029	2.049	2.071	2.038	2.060	2.027	2.051	1.996	2.008	2.069	2.055	2.056	2.065	2.016	2.016	2.004	2.018	1.993	1.996	2.000	1.999
Fe^{3+}	0.01601	0.03403	0.04567	0.03781	0.000	0.000	0.000	0.000	0.024	0.000	0.006	0.000	0.000	0.000	0.000	0.000	0.000	0.000	0.000	0.000	0.000	0.000	0.000	0.000
Fe^{2+}	1.65054	1.75814	1.66735	1.74423	2.074	2.309	2.179	2.336	1.790	1.697	1.375	1.776	2.133	2.134	2.139	2.099	1.825	1.512	1.533	1.872	1.637	1.746	1.674	1.743
Mn	0.39083	0.23332	0.44168	0.19713	0.185	0.028	0.101	0.026	0.346	0.069	0.494	0.039	0.091	0.080	0.065	0.077	0.081	0.394	0.397	0.066	0.335	0.195	0.321	0.188
Mg	0.31144	0.33786	0.27133	0.35162	0.182	0.408	0.330	0.432	0.120	0.121	0.047	0.130	0.511	0.504	0.507	0.514	0.198	0.141	0.151	0.201	0.087	0.080	0.085	0.079
Ca	0.63004	0.64424	0.58935	0.67172	0.481	0.167	0.330	0.128	0.671	1.043	1.084	1.044	0.202	0.226	0.193	0.225	0.878	0.938	0.908	0.847	0.916	0.958	0.890	0.973
X_{alm}	0.54	0.57	0.54	0.57	0.71	0.79	0.74	0.80	0.59	0.55	0.45	0.59	0.71	0.71	0.68	0.69	0.61	0.50	0.51	0.62	0.53	0.57	0.54	0.58
X_{prp}	0.10	0.11	0.09	0.11	0.06	0.14	0.11	0.15	0.04	0.04	0.02	0.04	0.17	0.17	0.16	0.17	0.07	0.05	0.05	0.07	0.03	0.03	0.03	0.03
X_{sps}	0.13	0.08	0.14	0.06	0.06	0.01	0.03	0.01	0.11	0.02	0.16	0.01	0.03	0.03	0.02	25.00	0.03	0.13	0.13	0.02	0.11	0.06	0.10	0.06
X_{grs}	0.21	0.21	0.19	0.22	0.16	0.06	0.11	0.04	0.22	0.34	0.36	0.35	0.07	0.07	0.06	0.07	0.29	0.31	0.30	0.28	0.30	0.31	0.29	0.32
X_{Mg}	0.16	0.16	0.14	0.16	0.08	0.15	0.13	0.16	0.06	0.07	0.03	0.07	0.19	0.19	0.19	0.20	0.10	0.09	0.09	0.10	0.05	0.04	0.05	0.04

Table 4: Representative biotite, plagioclase, muscovite, amphibole and epidote-clinozoisite compositions

Mineral	Biotite						Plagioclase								Muscovite					Amphibole			Epidote-clinozoisite
Sample	ST257	S8d	S174a	UL250	AR186		ST257	S8d	S174a		UL250		AR186		S8d		S17	UL250	AR186	ST254b		ST257	ST254b
									core	rim	core	rim	core	rim						Amp1	Amp2		
Wt%																							
SiO_2	37.32	35.36	36.54	35.97	36.32	36.33	62.84	63.59	62.61	62.20	62.12	63.27	64.53	64.23	46.33	46.68	46.69	48.33	47.64	47.09	45.71	42.39	38.44
TiO_2	1.84	1.66	2.82	2.61	3.00	2.62	0.03	0.04	0.01	0.00	0.00	0.00	0.00	0.00	0.75	0.70	0.84	0.94	0.60	0.48	0.59	0.73	0.10
Cr_2O_3	0.06	0.01	0.01	0.00	0.01	0.04	0.00	0.00	0.00	0.00	0.00	0.00	0.00	0.05	0.02	0.00	0.02	0.02	0.00	0.25	0.07	0.06	0.05
Al_2O_3	17.33	18.61	17.80	17.13	16.20	16.70	23.48	22.97	23.58	24.52	23.71	23.03	18.97	22.17	34.15	34.92	34.06	32.99	29.44	11.61	13.34	16.26	28.23
FeO_{TOT}	18.46	21.17	26.32	20.97	29.68	30.00	0.00	0.02	0.10	0.18	0.04	0.14	0.07	0.00	1.69	1.53	1.40	1.63	4.33	14.61	15.25	17.72	7.53
MnO	0.12	0.03	0.11	0.09	0.42	0.34	0.01	0.05	0.02	0.01	0.00	0.00	0.00	0.04	0.06	0.01	0.02	0.00	0.05	12.54	11.58	0.19	0.15
MgO	12.52	11.11	6.77	8.27	4.03	4.35	0.00	0.01	0.00	0.01	0.00	0.00	0.00	0.00	1.23	0.94	1.44	1.61	1.50	10.91	10.70	8.72	0.04
CaO	0.07	0.00	0.02	0.00	0.00	0.04	3.76	3.67	3.99	4.70	5.09	4.05	0.00	2.44	0.00	0.00	0.00	0.00	0.00	1.84	2.04	10.08	22.51
Na_2O	0.25	0.26	0.07	0.11	0.03	0.05	9.09	9.20	8.24	8.62	9.09	9.82	0.51	9.90	0.98	0.95	1.11	0.76	0.00	0.27	0.29	2.35	0.03
K_2O	9.11	9.08	9.61	9.59	9.54	9.72	0.14	0.15	1.44	0.17	0.10	0.05	16.01	0.21	9.84	8.80	9.46	10.17	10.64	0.27	0.29	0.66	0.01
Total	97.08	97.28	100.07	94.74	99.23	100.19	99.34	99.70	99.99	100.41	100.15	100.36	100.09	99.05	95.05	94.53	95.04	96.46	94.20	99.87	99.88	99.17	97.09
Si	2.828	2.696	2.804	2.863	2.874	2.838	2.795	2.820	2.780	2.747	2.741	2.776	2.854	2.857	3.086	3.138	3.112	3.187	3.261	6.620	6.445	6.114	3.000
Ti	0.105	0.095	0.163	0.156	0.179	0.154	0.001	0.001	0.000	0.000	0.000	0.000	0.000	0.000	0.054	0.035	0.042	0.047	0.031	0.050	0.063	0.079	0.006
Cr	0.003	0.000	0.001	0.000	0.000	0.002	0.000	0.000	0.000	0.000	0.000	0.000	0.002	0.001	0.001	0.000	0.001	0.001	0.000	0.028	0.008	0.007	0.003
Al	1.548	1.673	1.610	1.607	1.511	1.538	1.231	1.201	1.234	1.276	1.233	1.191	1.161	1.154	2.613	2.767	2.676	2.564	2.375	1.924	2.217	2.764	2.597
Fe^{3+}	0.000	0.000	0.000	0.000	0.000	0.000	0.000	0.000	0.000	0.000	0.001	0.005	0.000	0.001	0.108	0.000	0.000	0.000	0.000	0.872	0.915	0.947	0.395
Fe^{2+}	1.170	1.350	1.689	1.396	1.964	1.960	0.003	0.001	0.004	0.007	0.000	0.000	0.000	0.000	0.026	0.086	0.078	0.090	0.248	0.846	0.883	1.190	0.096
Mn	0.008	0.002	0.007	0.006	0.028	0.022	0.000	0.002	0.001	0.000	0.000	0.000	0.002	0.001	0.001	0.000	0.001	0.000	0.003	0.034	0.035	0.023	0.010
Mg	1.414	1.263	0.774	0.981	0.475	0.506	0.000	0.001	0.000	0.001	0.000	0.000	0.000	0.000	0.108	0.094	0.143	0.159	0.153	2.627	2.434	1.875	0.005
Ca	0.005	0.000	0.002	0.000	0.000	0.004	0.179	0.174	0.190	0.222	0.241	0.190	0.116	0.106	0.000	0.000	0.000	0.000	0.000	1.643	1.616	1.558	1.882
Na	0.037	0.038	0.011	0.017	0.005	0.007	0.784	0.791	0.709	0.738	0.778	0.835	0.853	0.864	0.046	0.124	0.143	0.097	0.000	0.501	0.558	0.657	0.005
K	0.881	0.883	0.941	0.974	0.963	0.969	0.008	0.008	0.082	0.010	0.006	0.003	0.012	0.018	0.956	0.755	0.804	0.855	0.929	0.049	0.053	0.122	0.001
X_{Mg}	0.547	0.483	0.314	0.413	0.195	0.205																	
An %							18	18	19	23	24	19	12	10									